Electronic Supplementary Material (ESI) for Dalton Transactions.

Vapochromic Behavior of a Gold(I)-Lead(II) complex as a VOC Sensor

Sonia Moreno, David Royo, Abdel G. El-Hachimi, María Rodríguez-Castillo, Miguel Monge, M. Elena Olmos* and José M. López-de-Luzuriaga*

Departamento de Química, Universidad de La Rioja, Centro de Investigación en Síntesis Química (CISQ), Complejo Científico-Tecnológico, 26006 – Logroño, Spain

Electronic Supplementary Information

I. Characterization of the complexes

II. Computational studies

I. Characterization of the complexes

1. ^{1}H NMR signal assignment

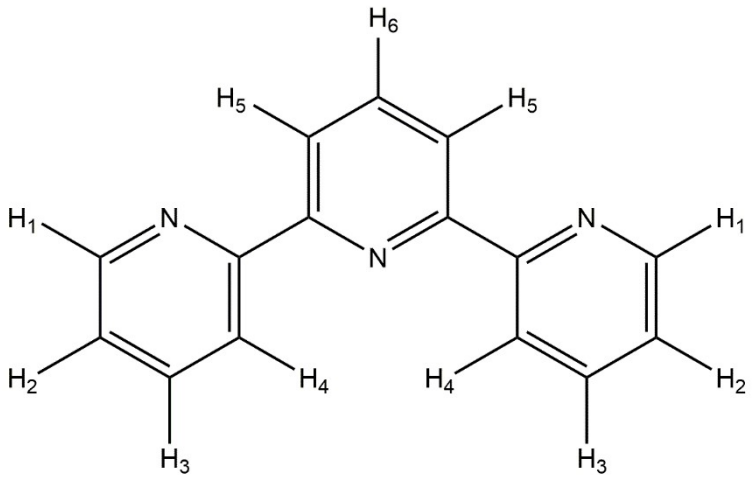

Figure S1. ^{1}H NMR signal assignment of terpyridine ligand.

2. IR spectra

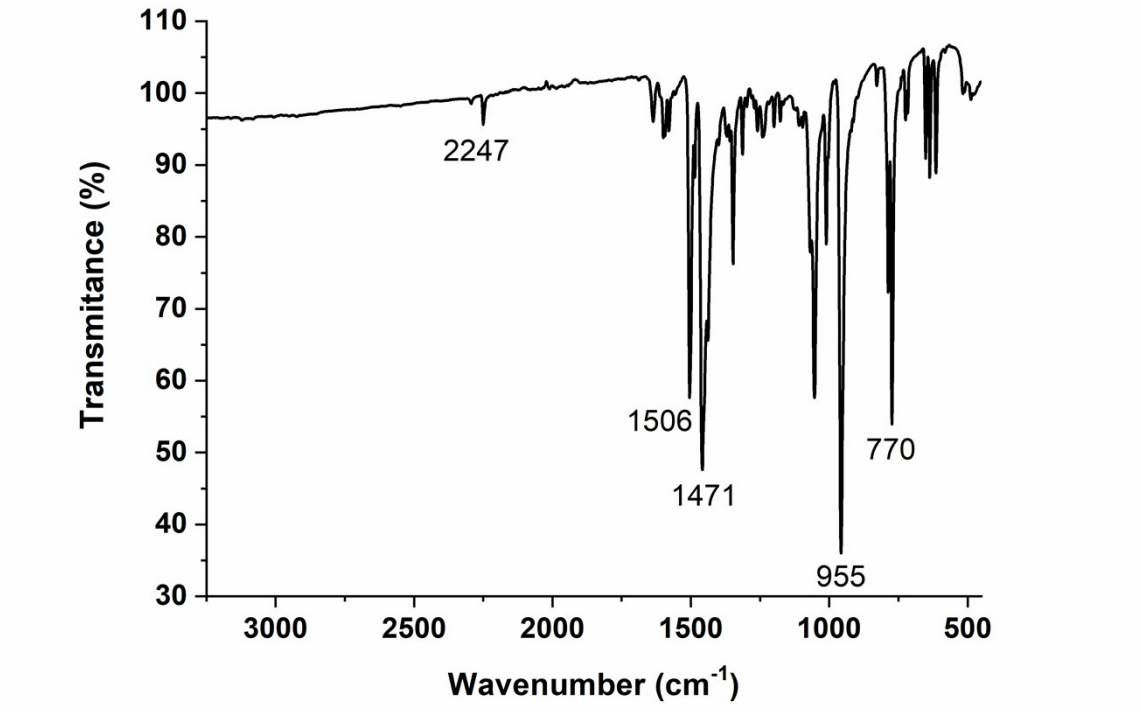

Figure S2. FT-IR spectrum of complex **2**.

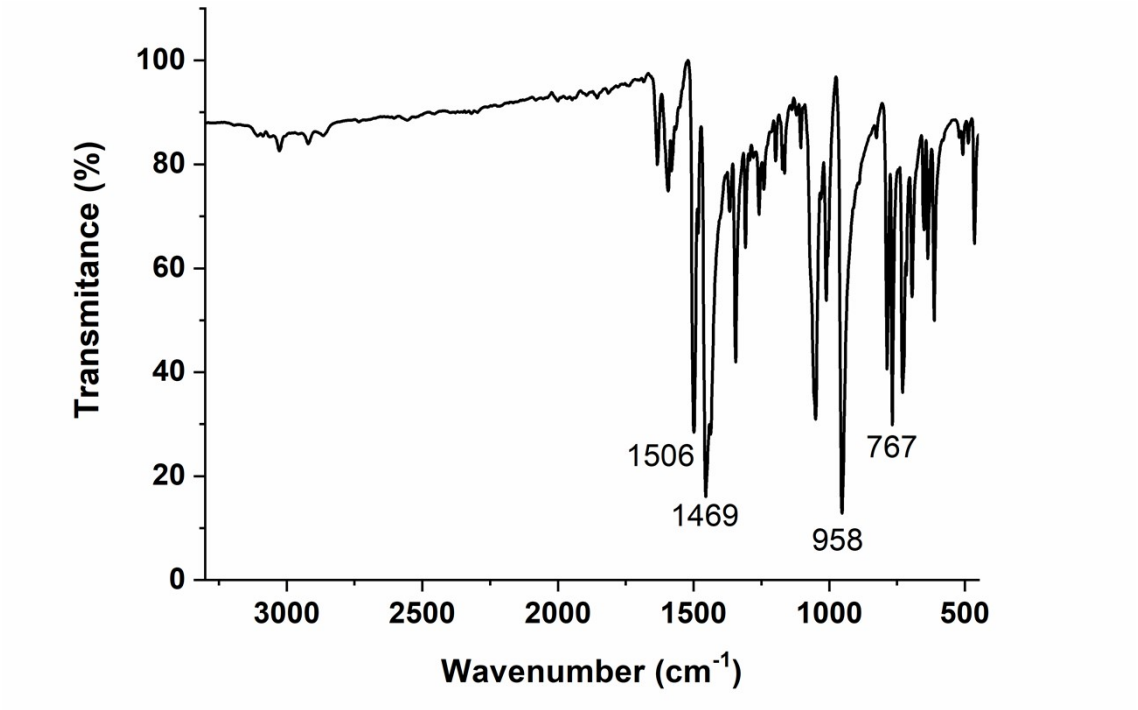

Figure S3. FT-IR spectrum of complex **3**.

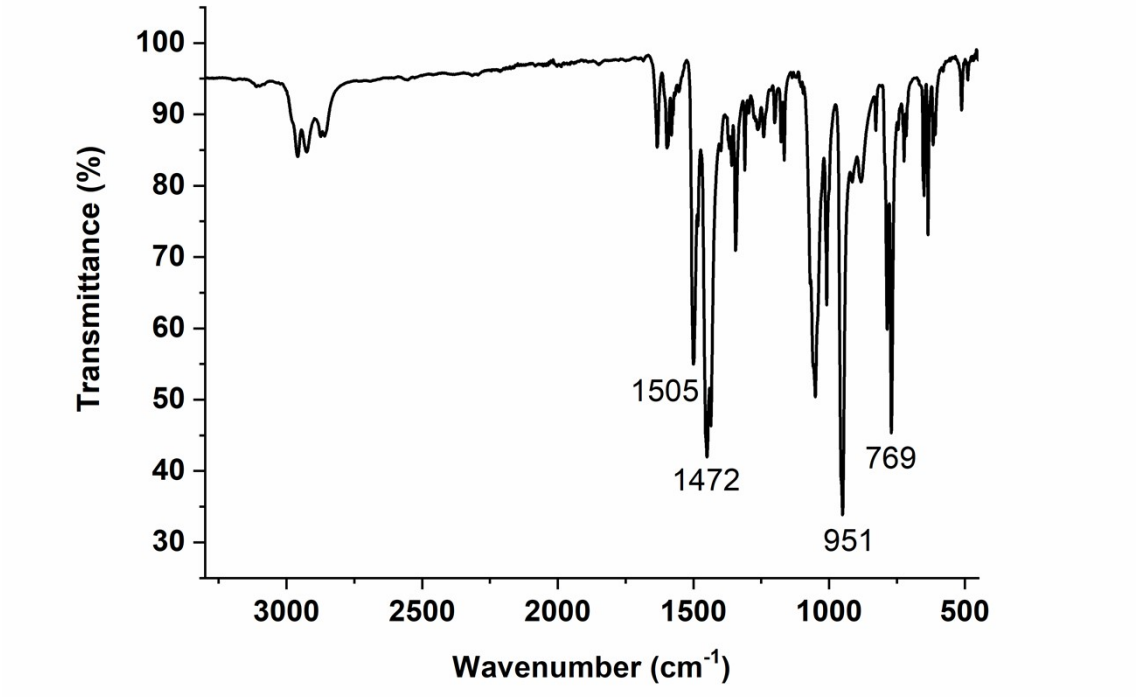

Figure S4. FT-IR spectrum of complex **4**.

3. ^{1}H NMR spectra (300 MHz, 298K)

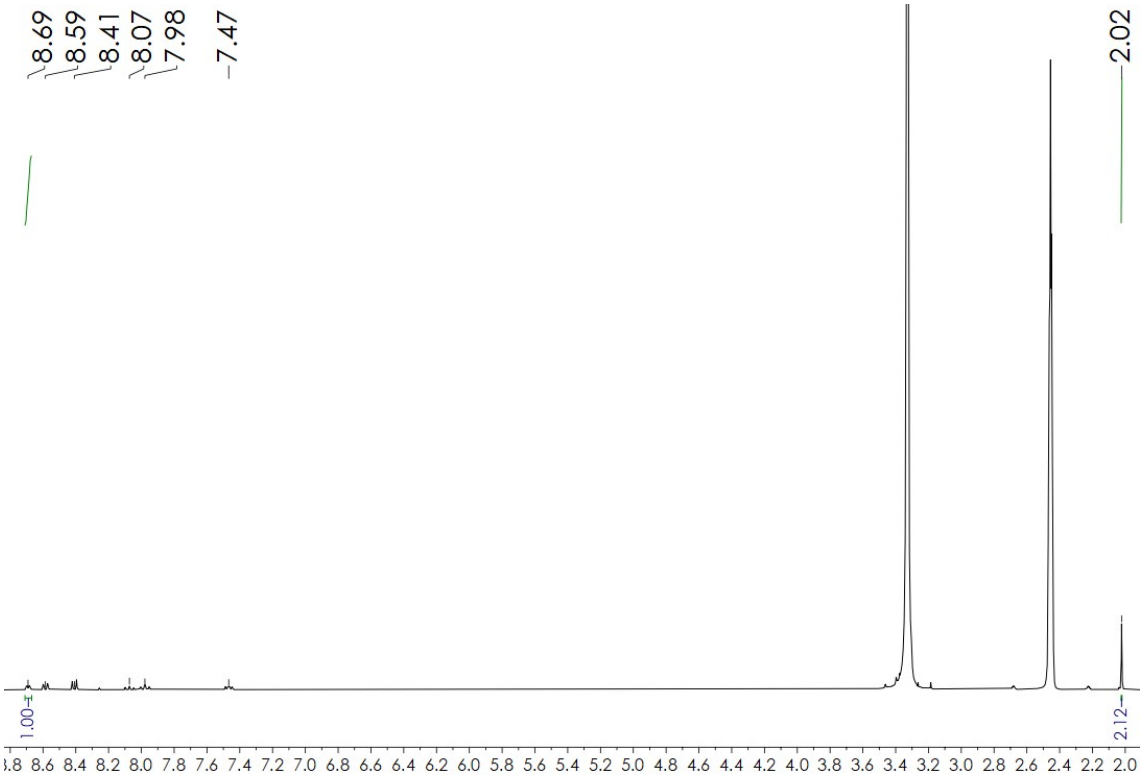

Figure S5. ^{1}H NMR spectrum of complex **2** in [D_6]-DMSO.

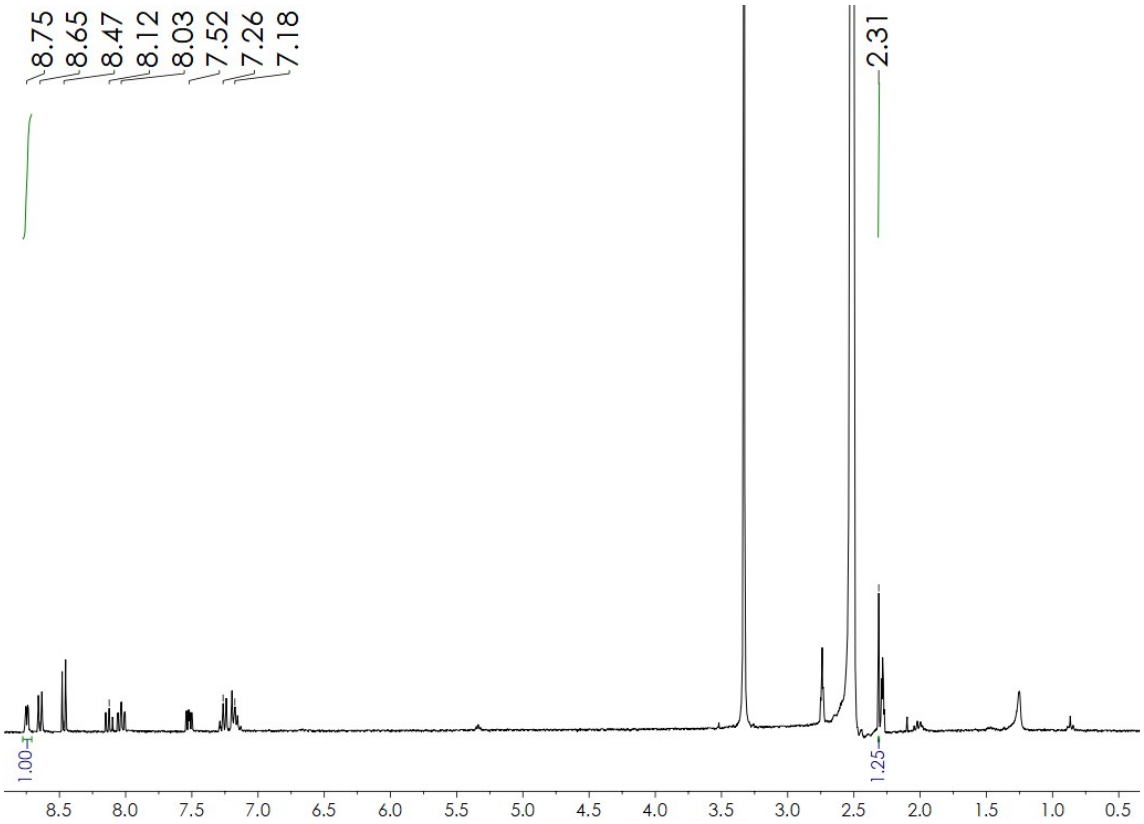

Figure S6. ^{1}H NMR spectrum of complex **3** in [D_6]-DMSO.

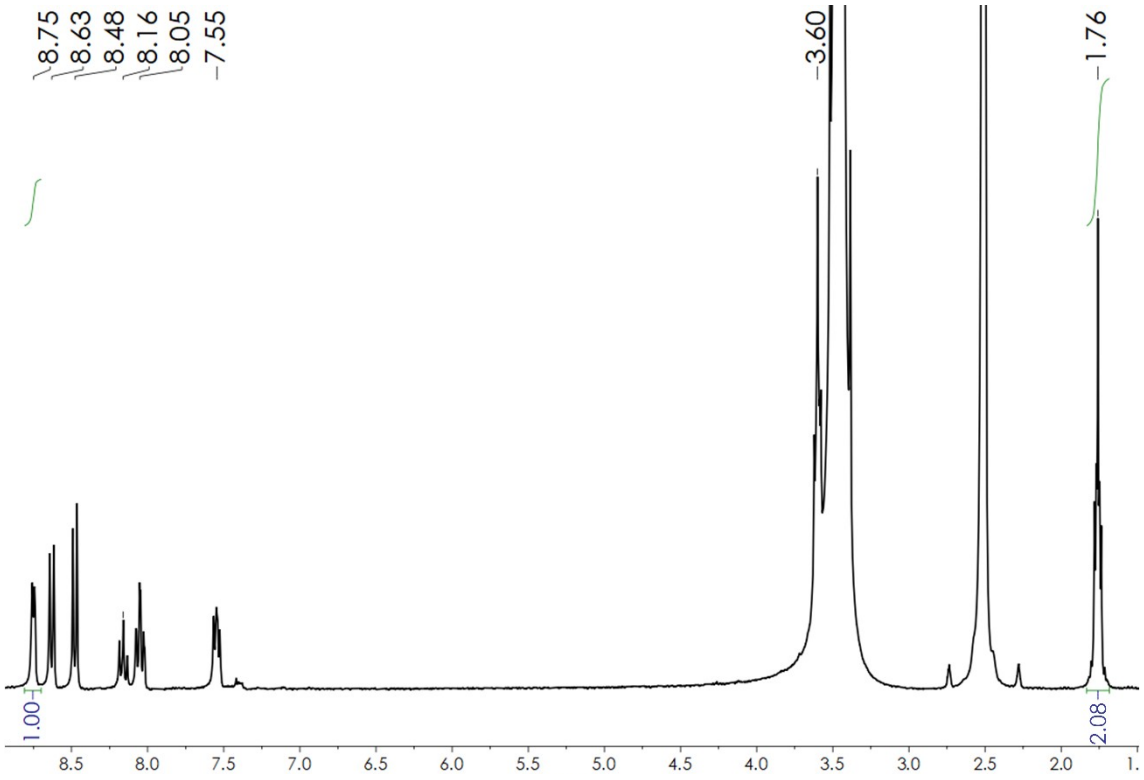

Figure S7. ^{1}H NMR spectrum of complex **4** in [D_6]-DMSO.

4. ^{19}F NMR spectra (282 MHz, 298K)

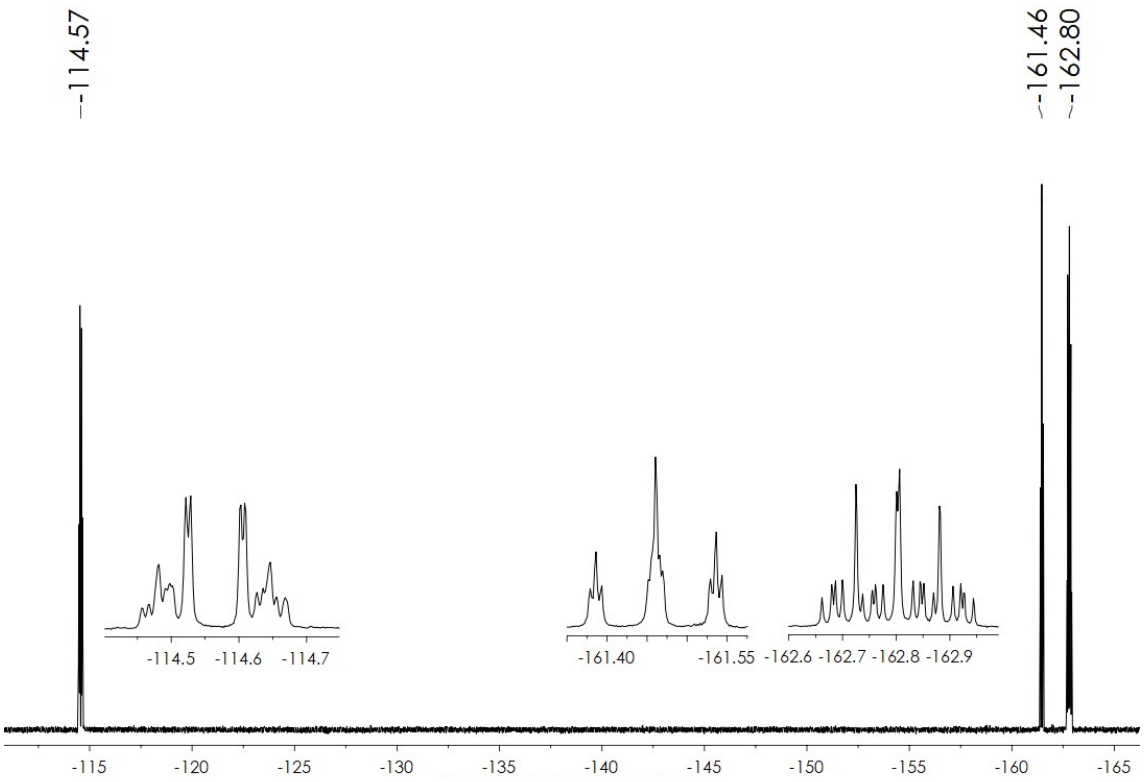

Figure S8. ^{19}F NMR spectrum of complex **2** in [D_6]-DMSO.

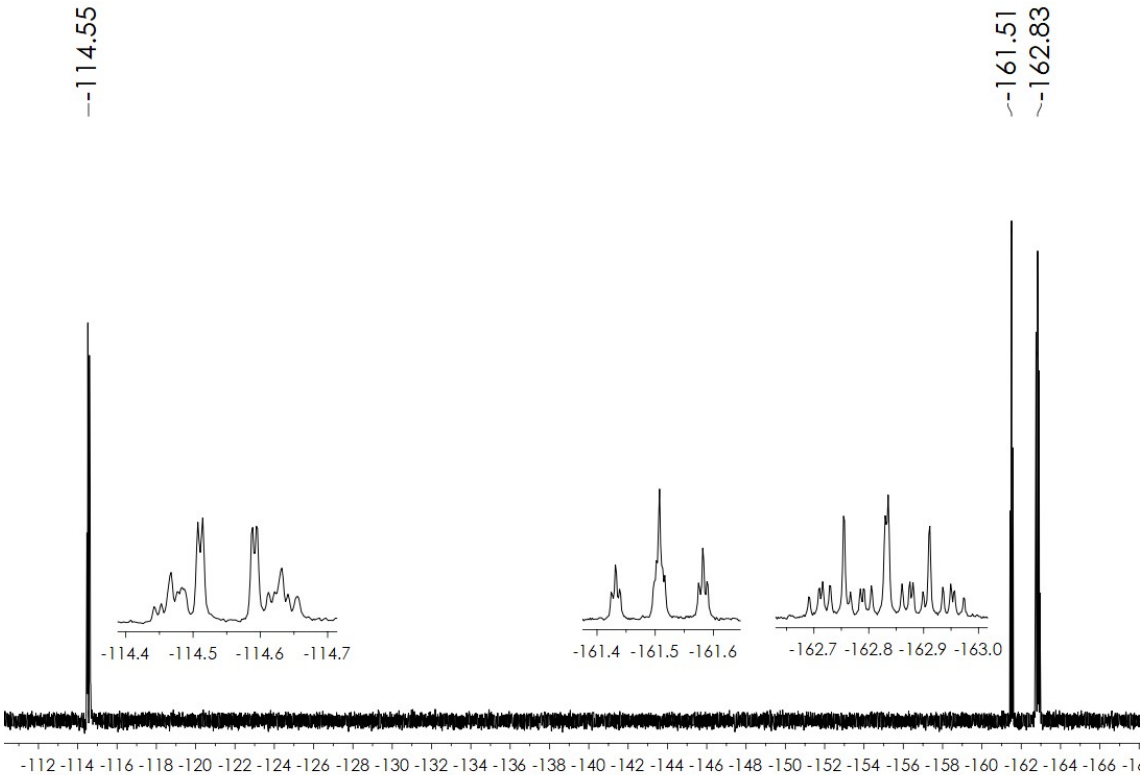

Figure S9. ^{19}F NMR spectrum of complex **3** in $[D_6]$-DMSO.

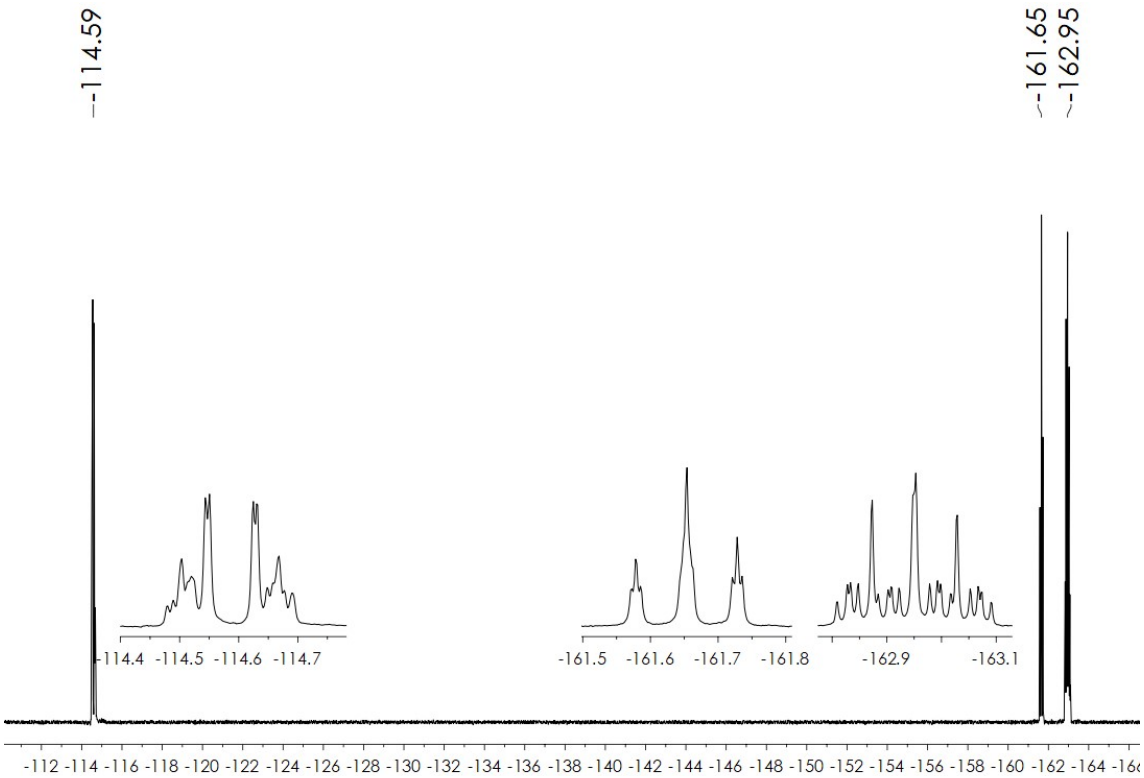

Figure S10. ^{19}F NMR spectrum of complex **4** in $[D_6]$-DMSO.

5. Single crystal analysis of compounds 2-4.

Table S1. Data collection and structure refinement details for **2-4**.

	2	**3**	**4**
Chemical Formula	$C_{39}H_{11}Au_2F_{20}N_3Pb\cdot2(C_2H_3N)$	$C_{39}H_{11}Au_2F_{20}N_3Pb\cdot C_7H_8$	$C_{39}H_{11}Au_2F_{20}N_3Pb\cdot2(C_4H_8O)$
Crystal habit	Yellow prism	Green prism	Yellow prism
Crystal size/mm	0.148x0.094x0.063	0.125x0.075x0.075	0.250x0.248x0.247
Crystal system	Triclinic	Monoclinic	Triclinic
Space group	P-1	Cc	P-1
a/Å	13.3822(11)	11.7382(5)	9.4745(10)
b/Å	16.9843(16)	25.0335(13)	14.2971(15)
c/Å	20.4646(18)	15.6517(6)	17.8209(17)
α/°	69.099(3)	90	107.528(3)
β/°	77.706(4)	105.334(3)	94.633(3)
γ/°	88.931(4)	90	93.988(4)
V/Å^3	4237.3(7)	4435.5(3)	2283.2(4)
Z	4	4	2
D_c/g cm^{-3}	2.482	2.388	2.395
M	1584.74	1594.76	1646.84
F(000)	2920	2944	1532
T/ºC	-100	-100	-100
2θmax/°	52	51	56
μ(Mo-*K*α)/mm^{-1}	11.001	10.509	10.215
No. refl. Measured	134396	28760	48068
No. unique refl.	16682	7888	10904
R_{int}	0.0507	0.0902	0.0405
$R[F>2\sigma(F)]$[a]	0.0357	0.0435	0.0230
$wR[F^2$, all refl.][b]	0.1024	0.0910	0.0462
No. of refl. Used [$F>2\sigma(F)$]	16682	7888	10904
No. of parameters	1271	645	670
No. of restrains	320	266	20
S [c]	1.080	1.002	1.059
Max. residual electron density/e·Å^{-3}	3.579	1.035	0.81

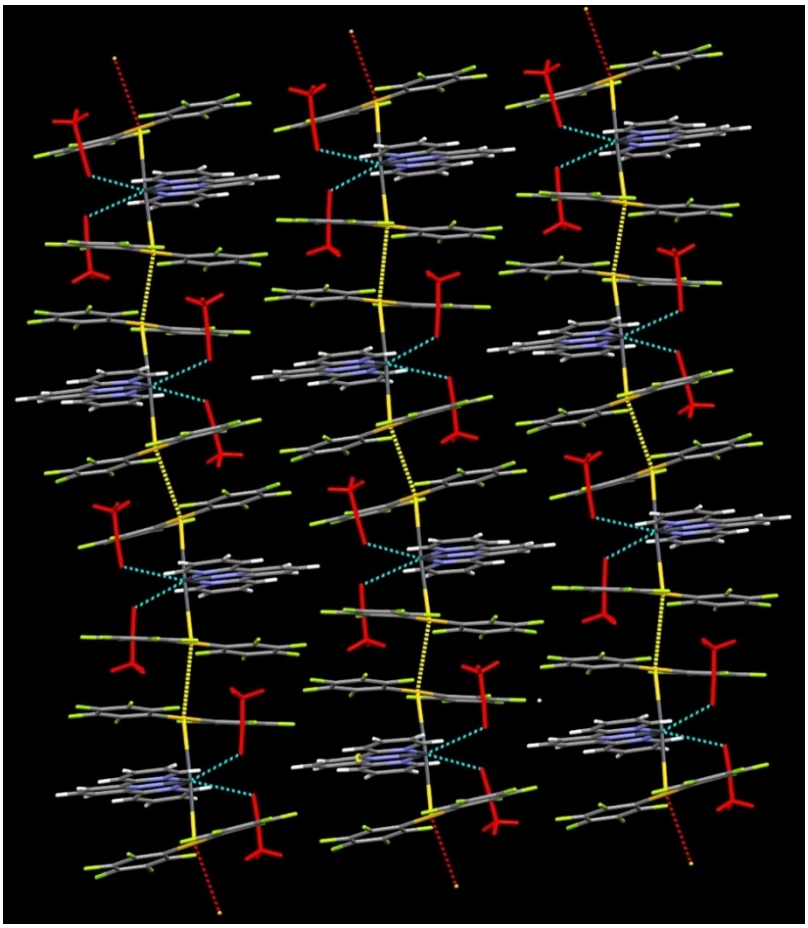

Figure S11. Crystal structure of **2** with the acetonitrile molecules in red.

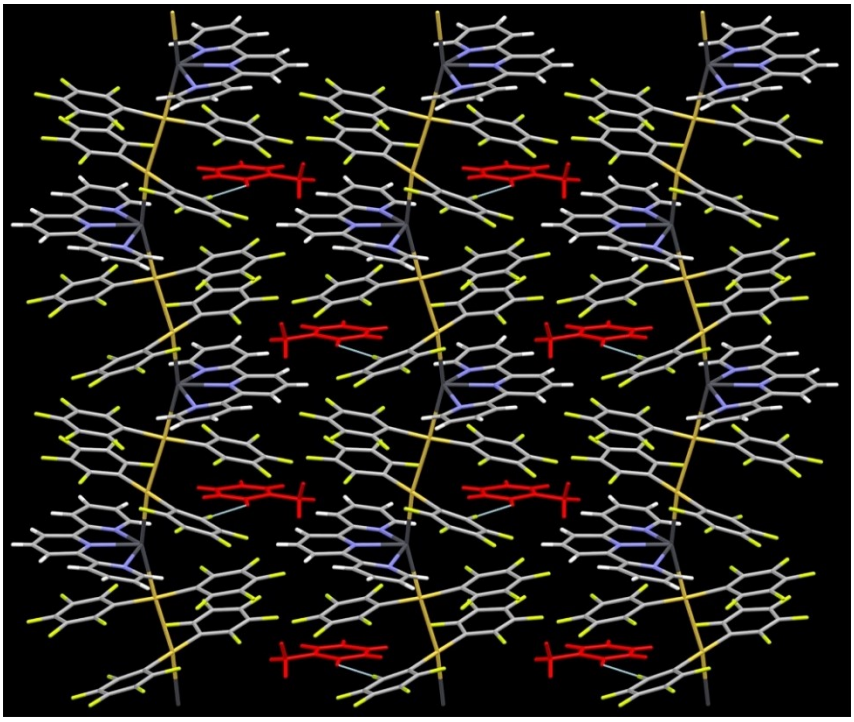

Figure S12. Crystal structure of **3** viewed down the crystallographic *x* axis with the toluene molecules in red.

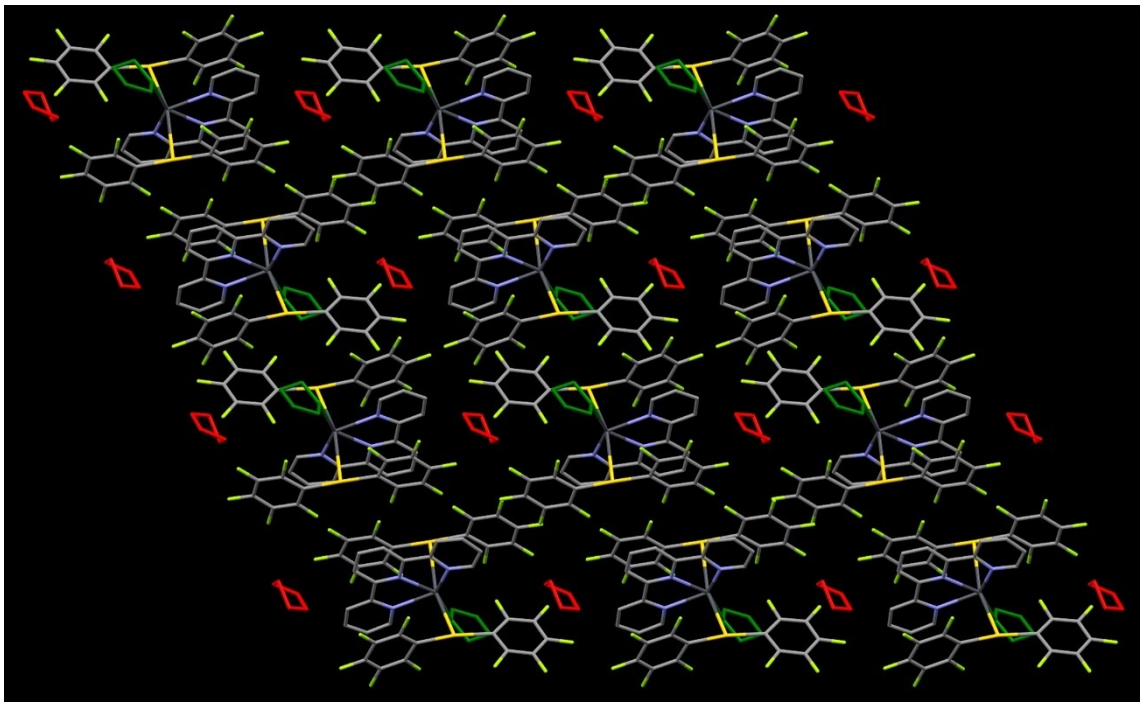

Figure S13. Crystal structure of **4** viewed down the crystallographic *x* axis with the coordinated THF molecules in green and the non-coordinated THF molecules in red. Hydrogen atoms have been omitted for calriry.

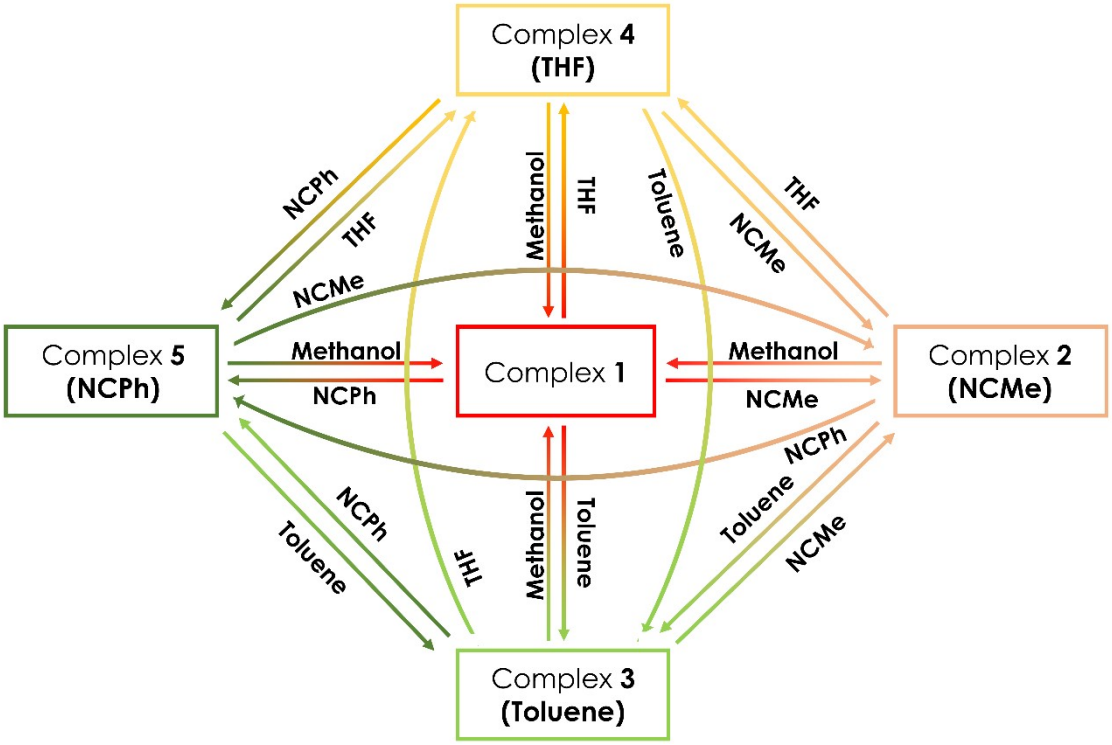

Figure S14. Schematic of the reversibility of compounds **1-5** through vapours of the different solvents.

6. Powder X-ray diffraction analysis.

X-ray diffraction measurements were carried out at the X-ray Diffraction and Fluorescence Analysis Service of the General Research Support Service of the University of Zaragoza. The data have been collected with a diffractometer "D-Max Rigaku, Ru300", provided with a Cu rotating anode. The diffractometer is operated at 40Kv and 80 mA and a graphite monochromator is used to select the Cu Kα radiation. Measurement conditions from 2theta 3º to 40º step=0.03 t=1s/step.

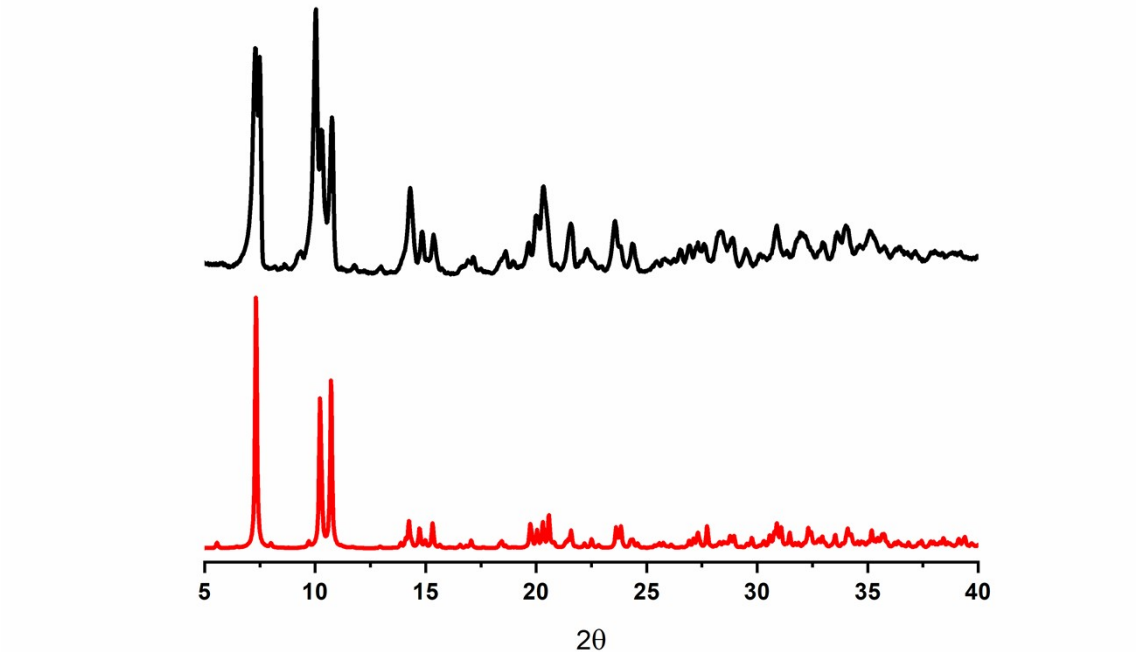

Figure S15. Theoretical (red) and experimental (black) X-ray powder pattern of complex **1**.

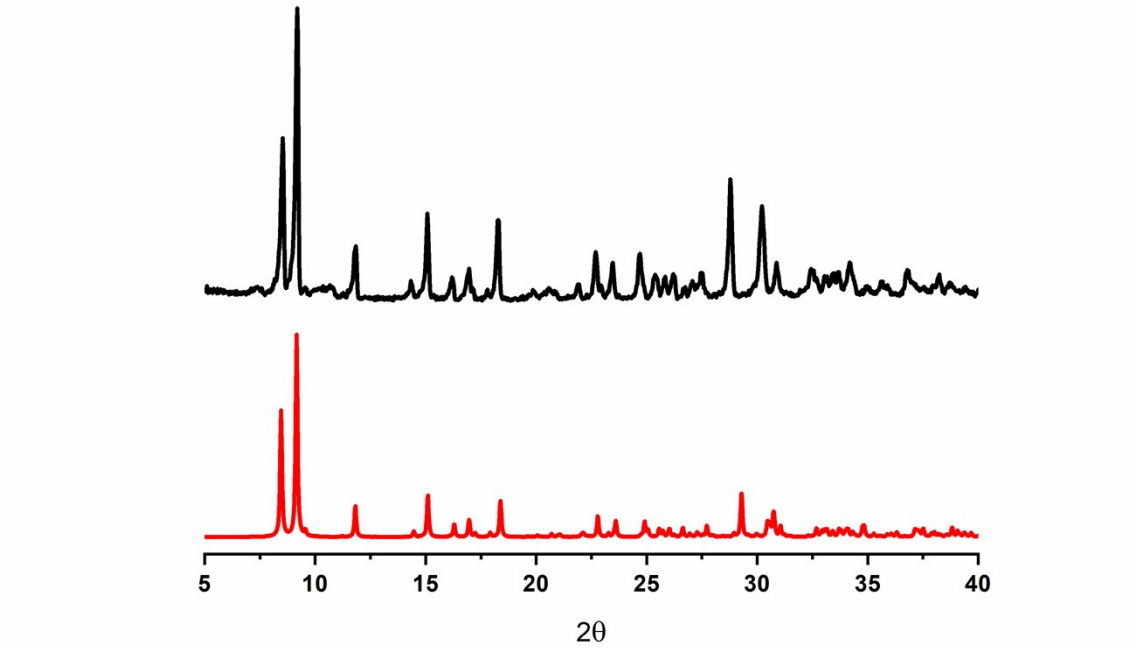

Figure S16. Theoretical (red) and experimental (black) X-ray powder pattern of complex **2**.

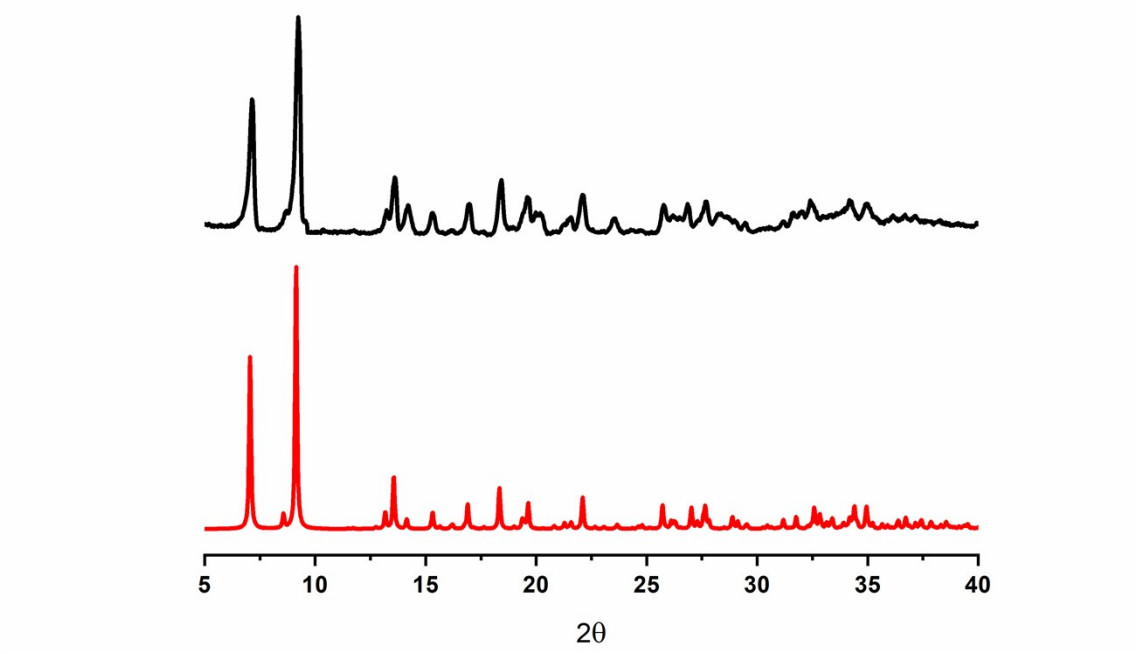

Figure S17. Theoretical (red) and experimental (black) X-ray powder pattern of complex **3**.

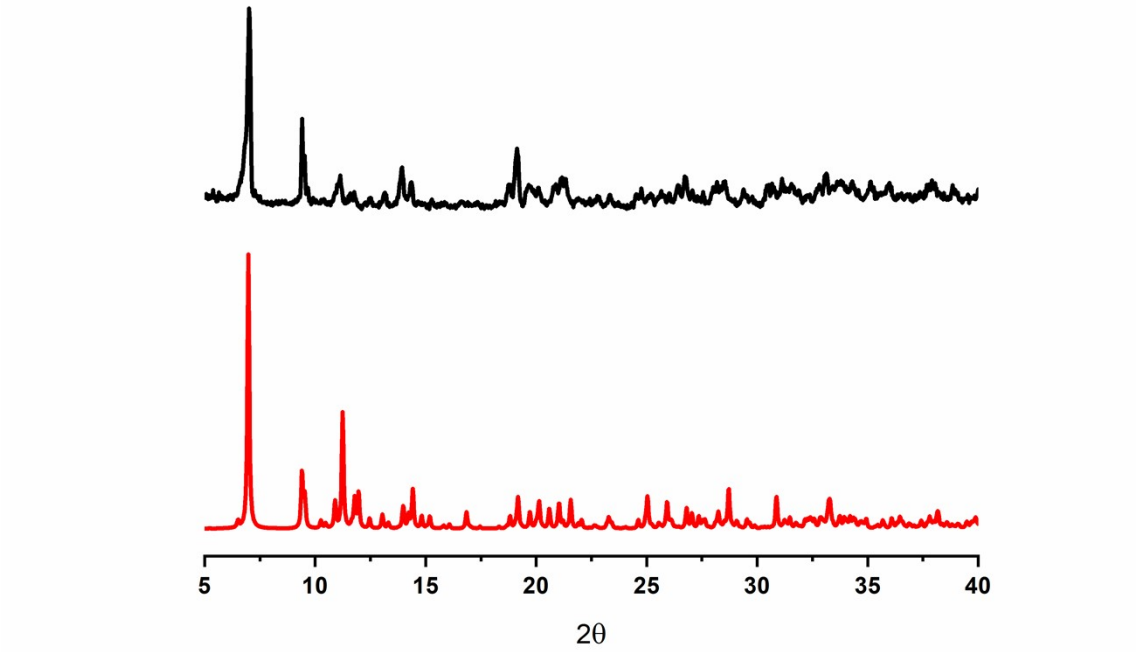

Figure S18. Theoretical (red) and experimental (black) X-ray powder pattern of complex **4**.

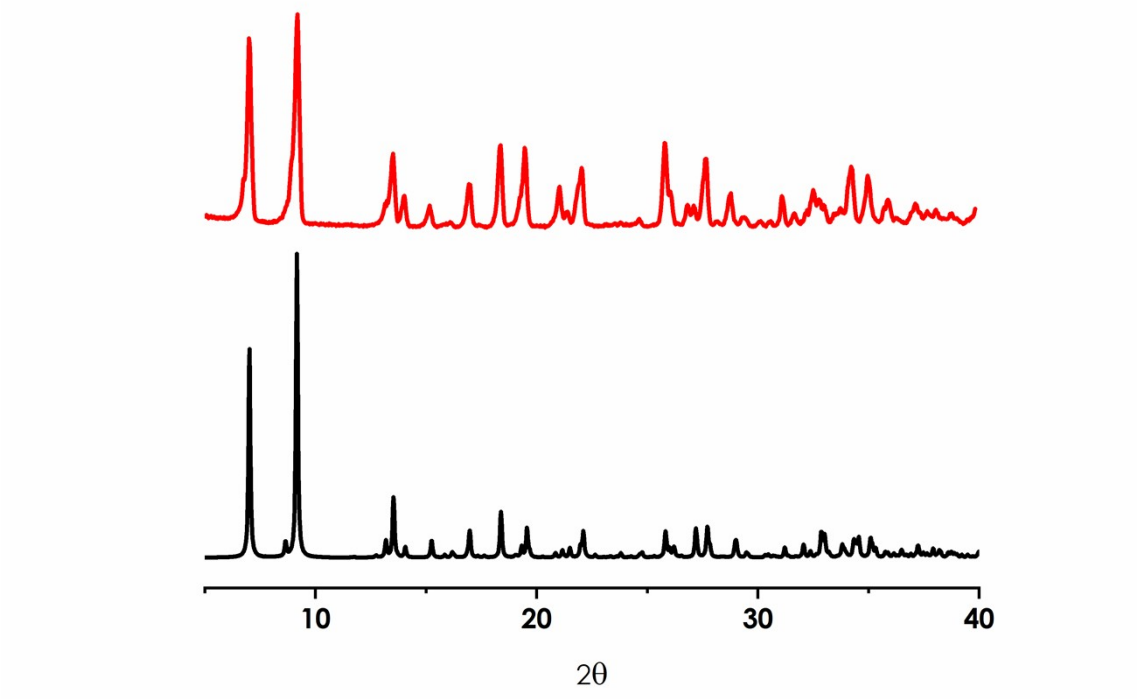

Figure S19. Theoretical (red) and experimental (black) X-ray powder pattern of complex **5**.

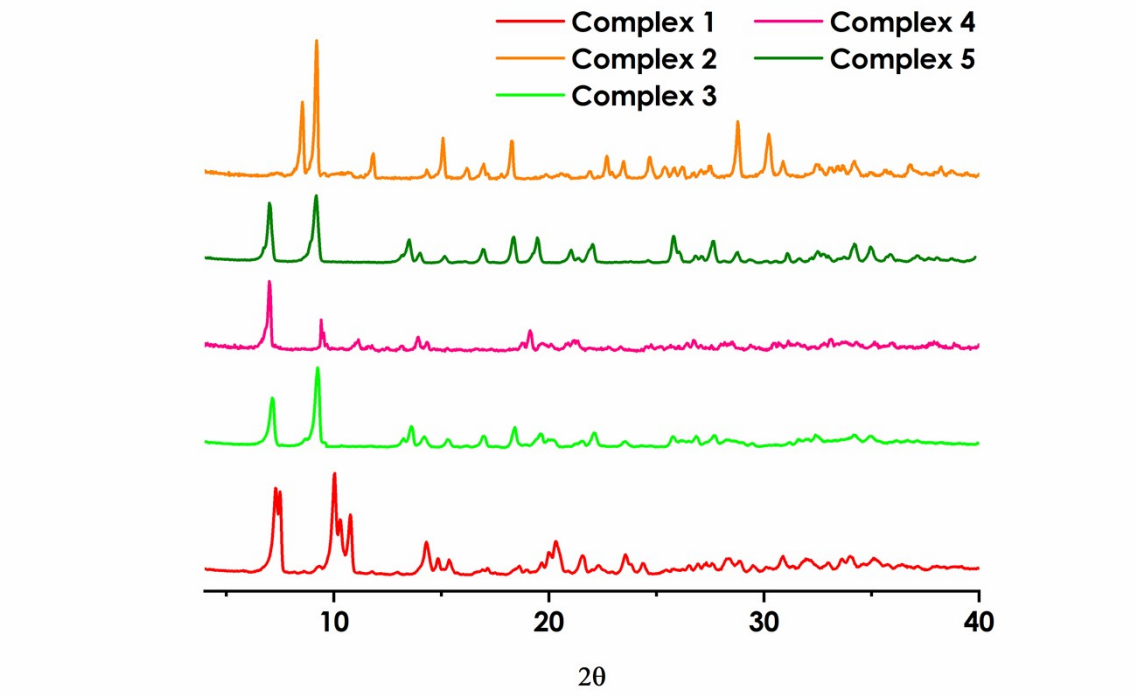

Figure S20. X-ray diffraction spectra of powder obtained by treatment of compound **1** (red) with acetonitrile (compound **2**, orange), toluene (compound **3**, light green), tetrahydrofuran (compound **4**, pink) and benzonitrile (compound **5**, dark green) vapours.

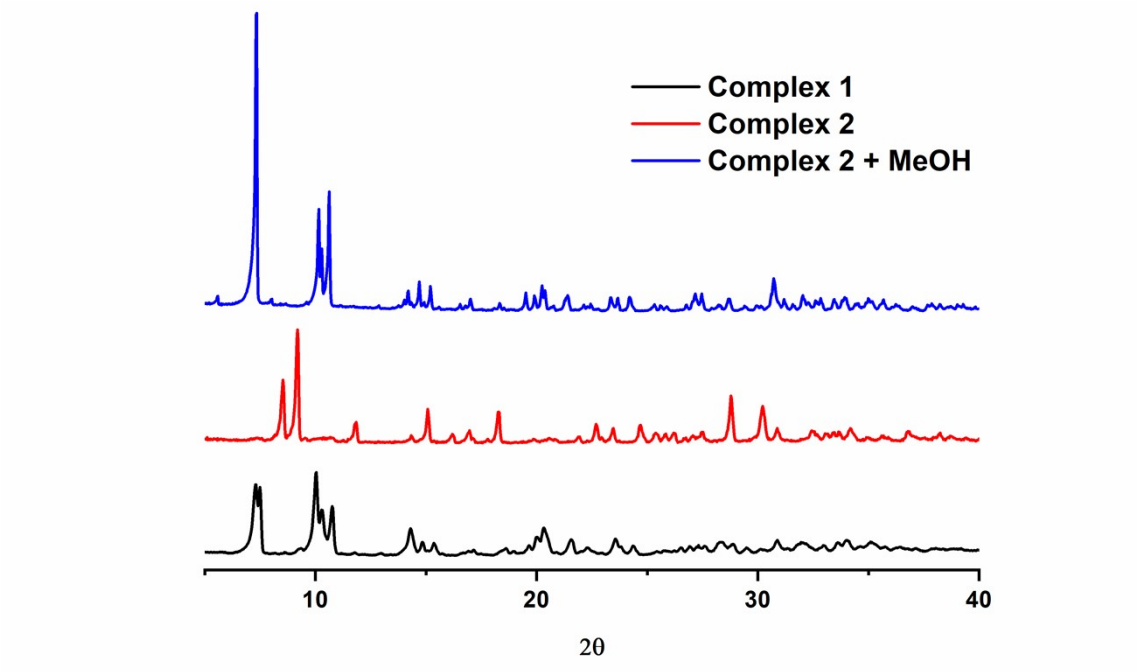

Figure S21. Experimental X-ray powder pattern of complex **1** (black), complex **2** (red) and complex **2** after contact with methanol (blue).

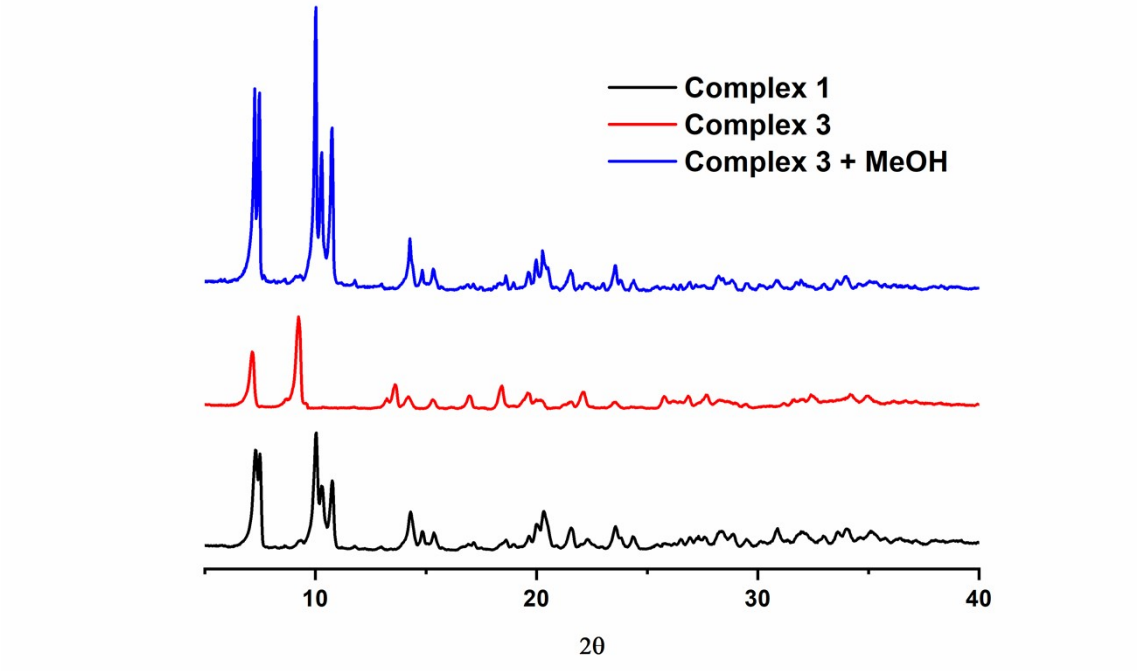

Figure S22. Experimental X-ray powder pattern of complex **1** (black), complex **3** (red) and complex **3** after contact with methanol (blue).

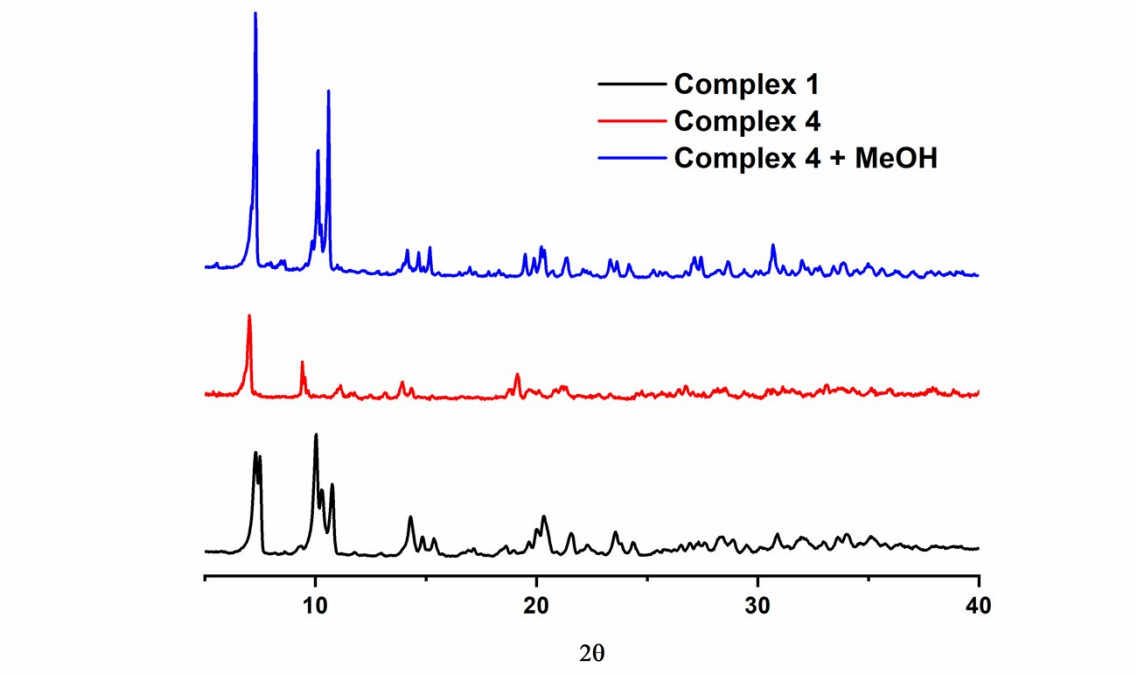

Figure S23. Experimental X-ray powder pattern of complex **1** (black), complex **4** (red) and complex **4** after contact with methanol (blue).

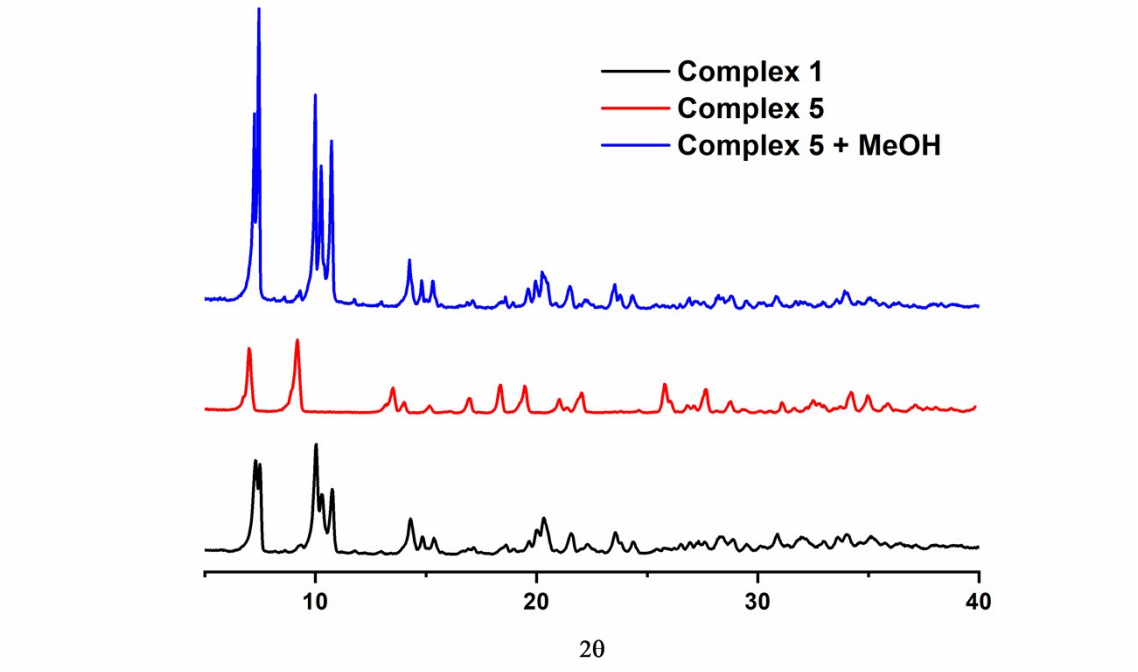

Figure S24. Experimental X-ray powder pattern of complex **1** (black), complex **5** (red) and complex **5** after contact with methanol (blue).

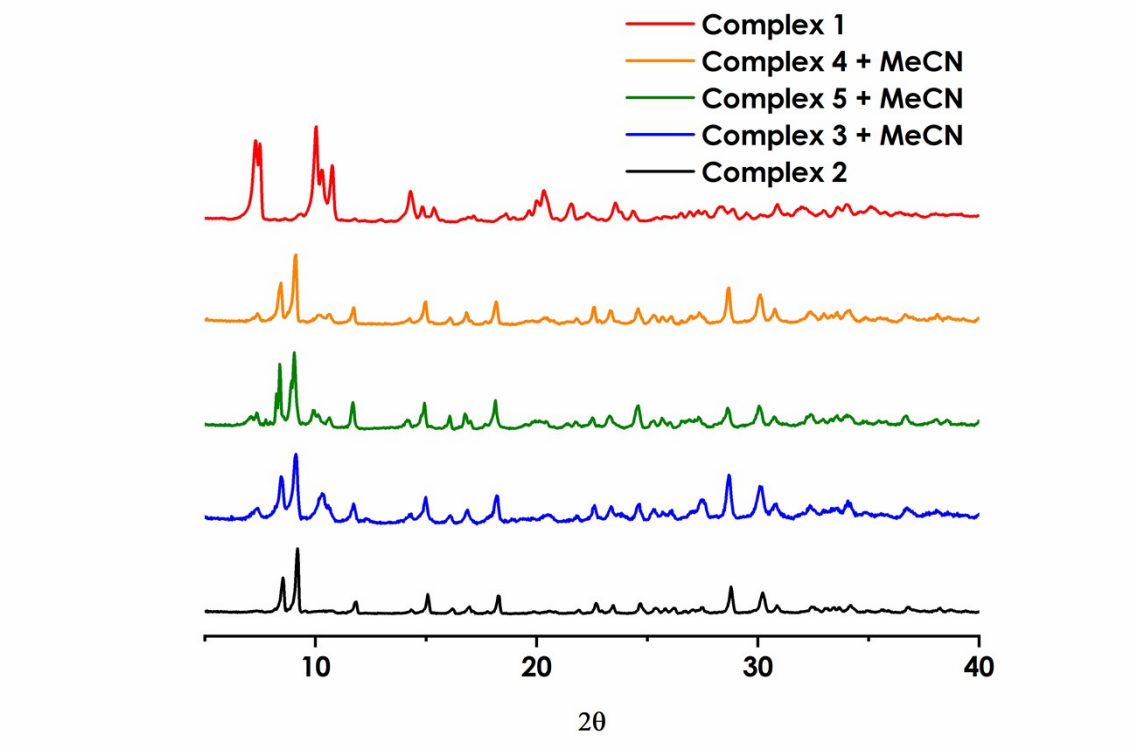

Figure S25. X-ray powder diffraction spectra of the conversion of compounds **3**, **4** and **5** to compound **2** upon exposure to acetonitrile vapours.

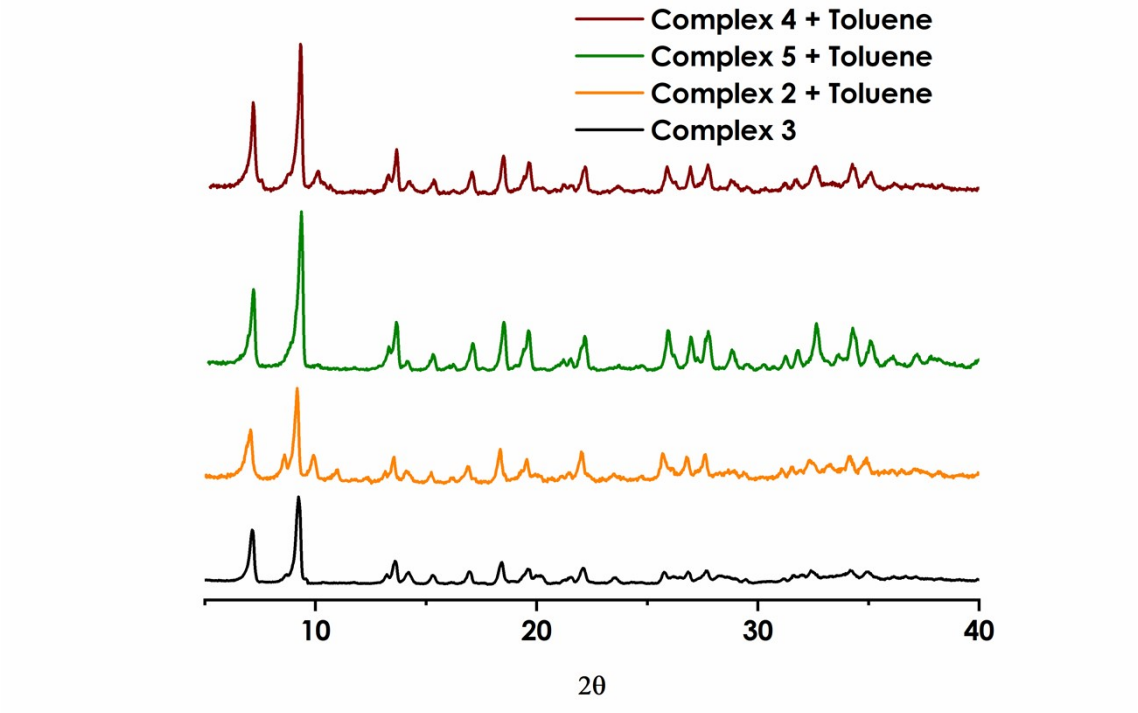

Figure S26. X-ray powder diffraction spectra of the conversion of compounds **2**, **4** and **5** to compound **3** upon exposure to toluene vapours.

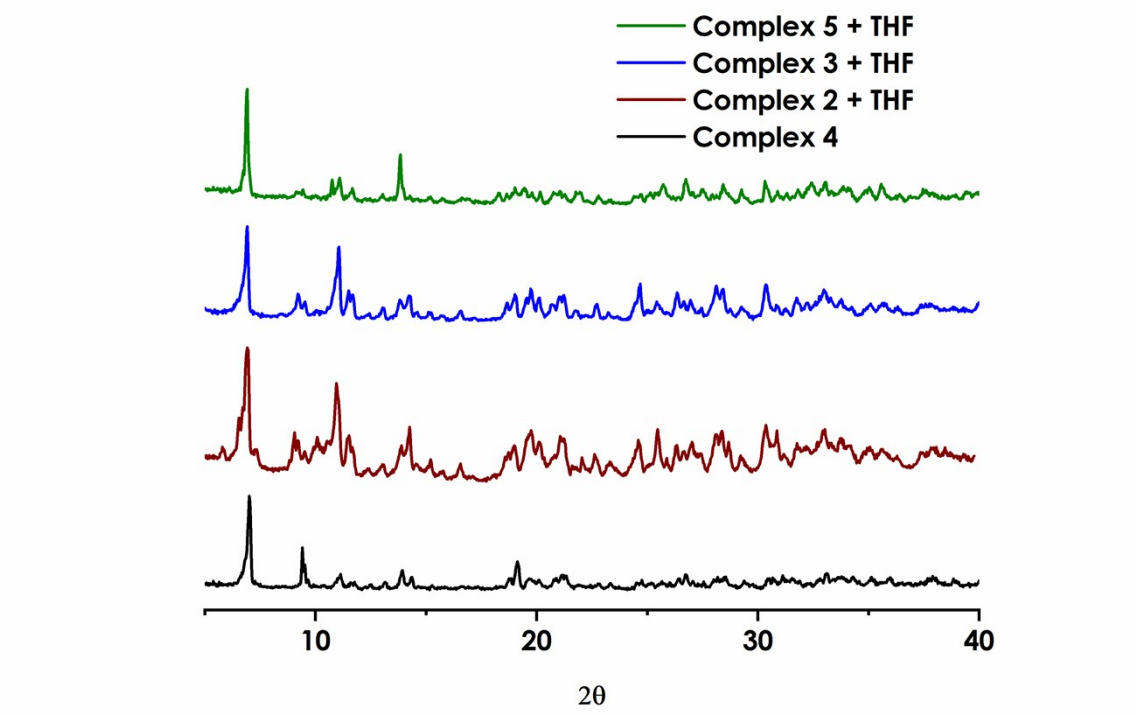

Figure S27. X-ray powder diffraction spectra of the conversion of compounds **2**, **3** and **5** to compound **4** upon exposure to toluene vapours.

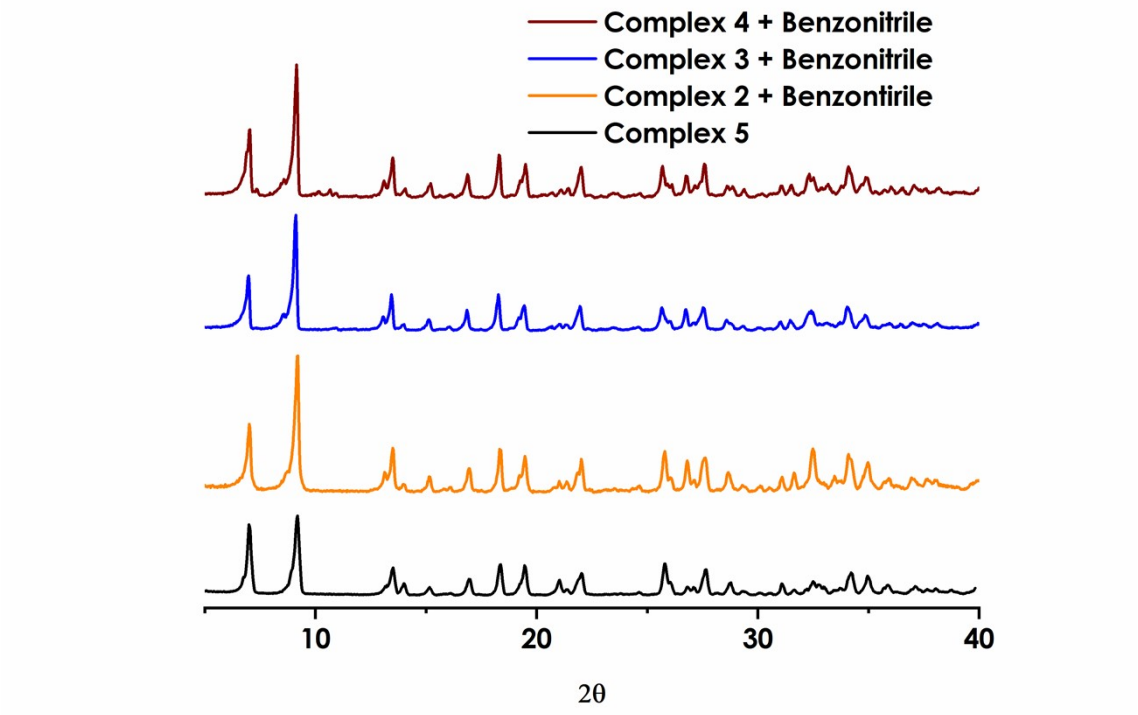

Figure S28. X-ray powder diffraction spectra of the conversion of compounds **2**, **3** and **4** to compound **5** upon exposure to toluene vapours.

7. Lifetimes

- **Complex 2:**

RT

Emission centred at 550 nm, excitation nanoled of 370 nm:

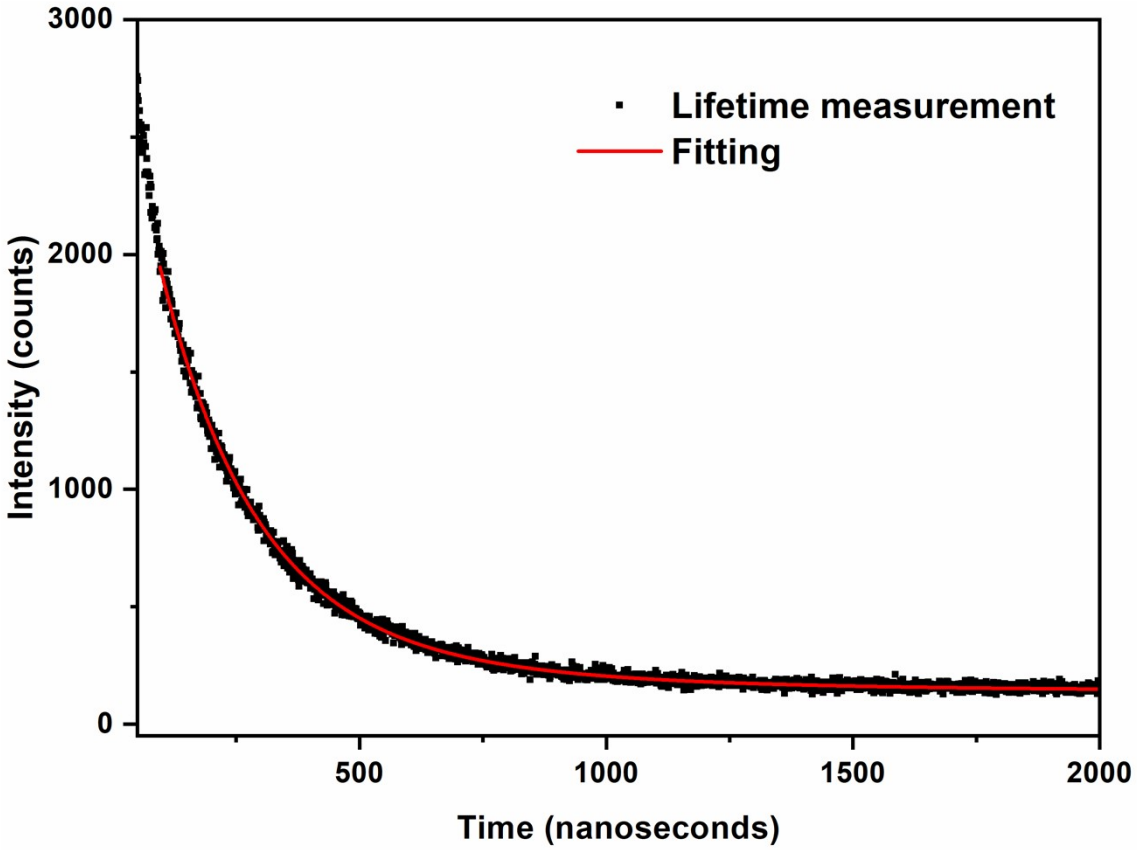

Figure S29. Lifetime decay for complex **2** at room temperature.

	Value	Std Dev		Value	Std Dev	Rel %
τ1	6.751E-7	1.243E-8	**B1**	1556.181	5.954128	68.15
τ2	1.963E-06	4.983E-08	**B2**	250.0792	2.838904	31.85
<τ>amp	0.853E-6					
Chisq	1.020		**A**	140.8187		
Shift	0					

77 K

Emission centred at 580 nm, excitation of 480 nm:

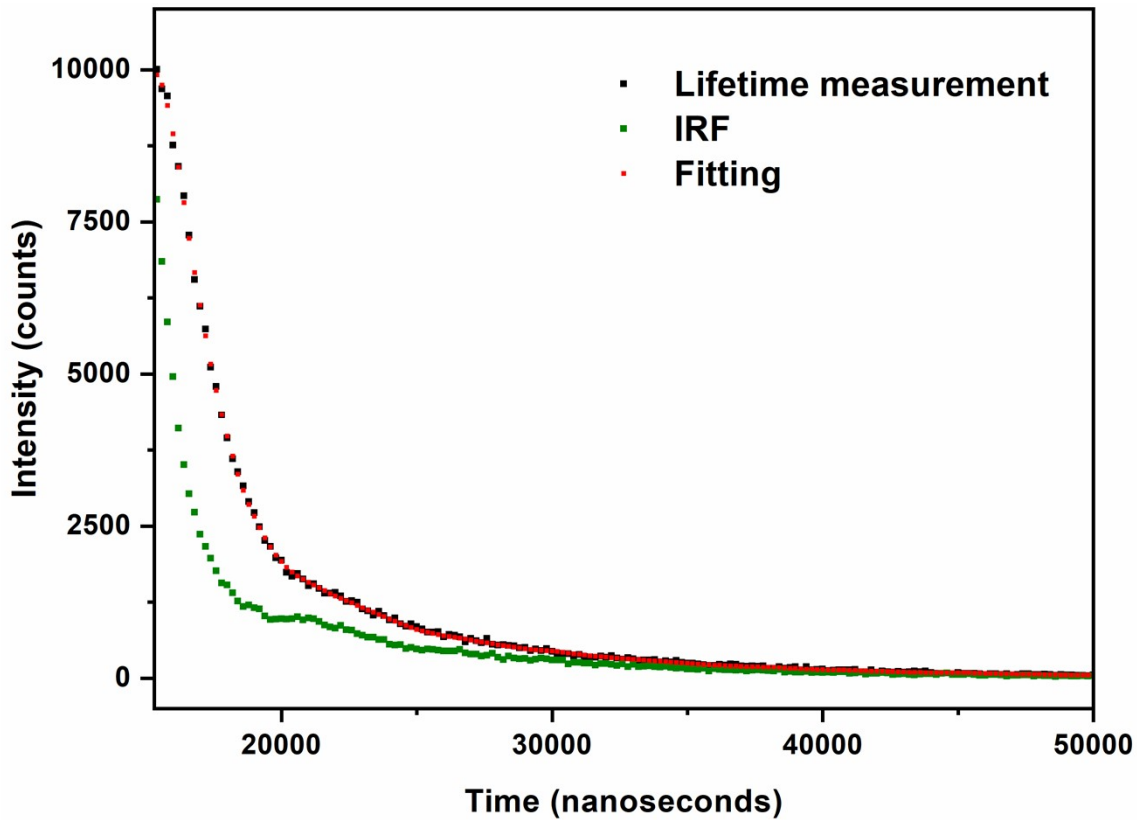

Figure S30. Lifetime decay for complex **2** at 77 K. *IRF (Instrumental Response Function) is used to detect the scattered light from the sample.

	Value	Std Dev		Value	Std Dev	Rel %
τ1	1.214E-6	1.024E-8	**B1**	2.206E-1	1.785E-3	100.00
<τ>amp	1.214E-6	1.024E-8				
Chisq	1.129		**A**	-7.617E-1		
Shift	1.474E-7					

- **Complex 3:**

RT

Emission centred at 770 nm, excitation nanoled of 560 nm:

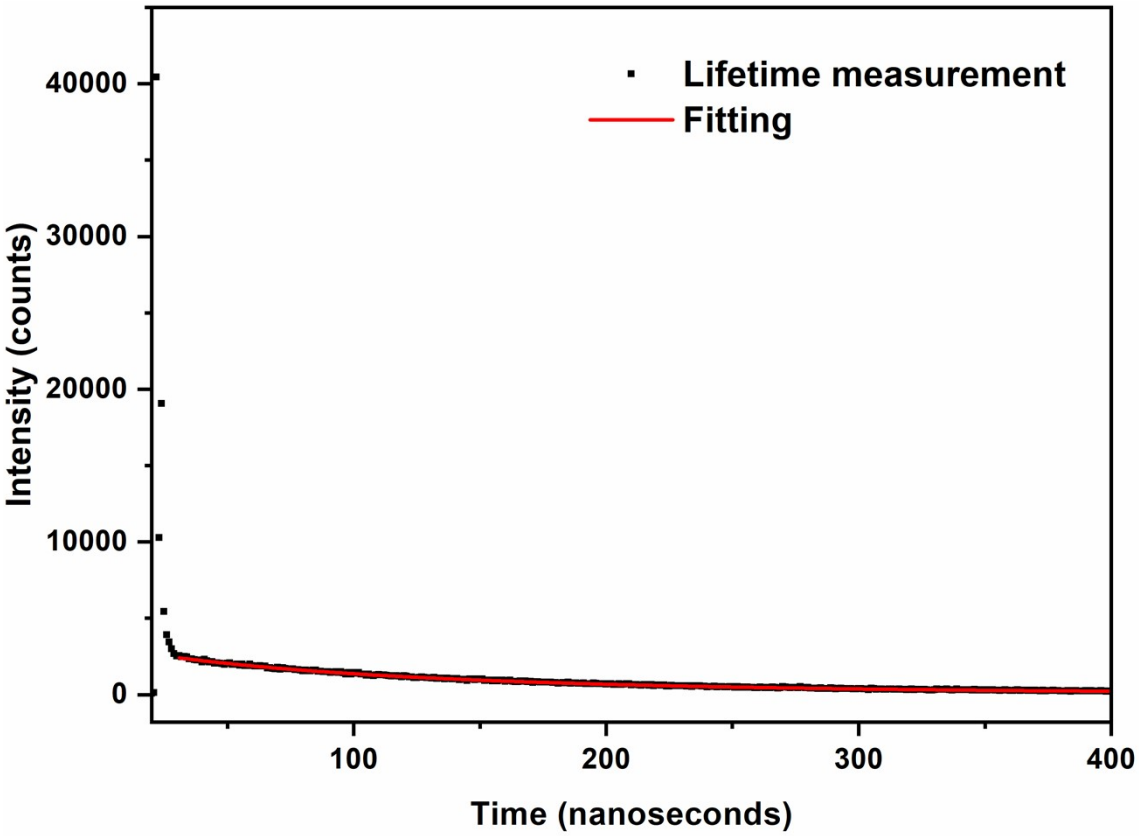

Figure S31. Lifetime decay for complex **3** at room temperature.

	Value	Std Dev		Value	Std Dev	Rel %
τ1	1.089E-7	1.105E-8	**B1**	605.4062	13.44573	12.45
τ2	2.676E-07	1.614E-09	**B2**	1732.089	6.953588	87.55
<τ>amp	0.226E-6					
Chisq	1.030		**A**	73.77539		
Shift	0					

77 K

Emission centred at 880 nm, excitation of 760 nm:

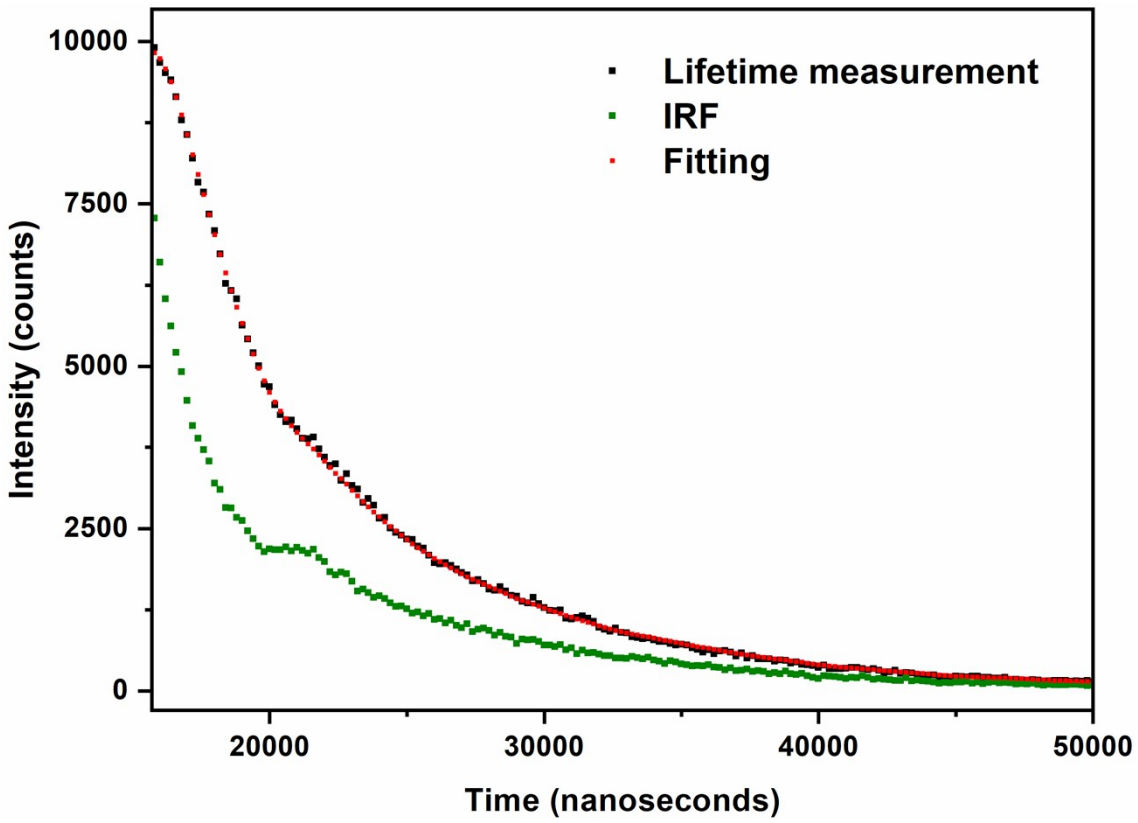

Figure S32. Lifetime decay for complex **3** at 77 K. *IRF (Instrumental Response Function) is used to detect the scattered light from the sample.

	Value	Std Dev		Value	Std Dev	Rel %
τ1	1.734E-6	1.313E-8	**B1**	1.686E-1	1.184E-3	100.00
<τ>amp	1.734E-6	1.313E-8				
Chisq	1.343		**A**	-1.713		
Shift	2.705E-7					

➢ **Complex 4**

RT

Emission centred at 530 nm, excitation nanoled of 390 nm:

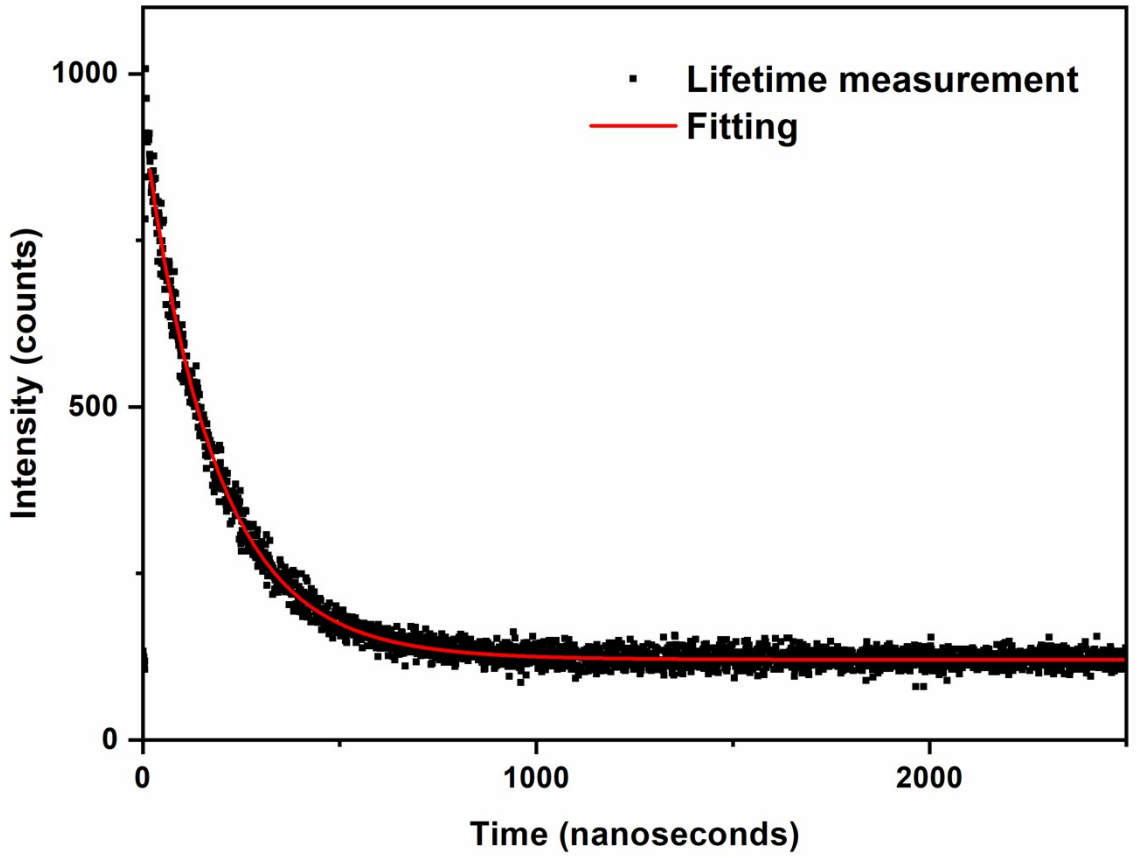

Figure S33. Lifetime decay for complex **4** at room temperature.

	Value	Std Dev		Value	Std Dev	Rel %
τ1	4.419E-6	9.308E-8	**B1**	51.36509	4.808246	11.92
τ2	2.455E-06	4.740E-08	**B2**	683.2266	7.126466	88.08
<τ>amp	2.592E-6					
Chisq	1.038		**A**	120.48		
Shift	0					

77 K

Emission centred at 550 nm, excitation of 425 nm:

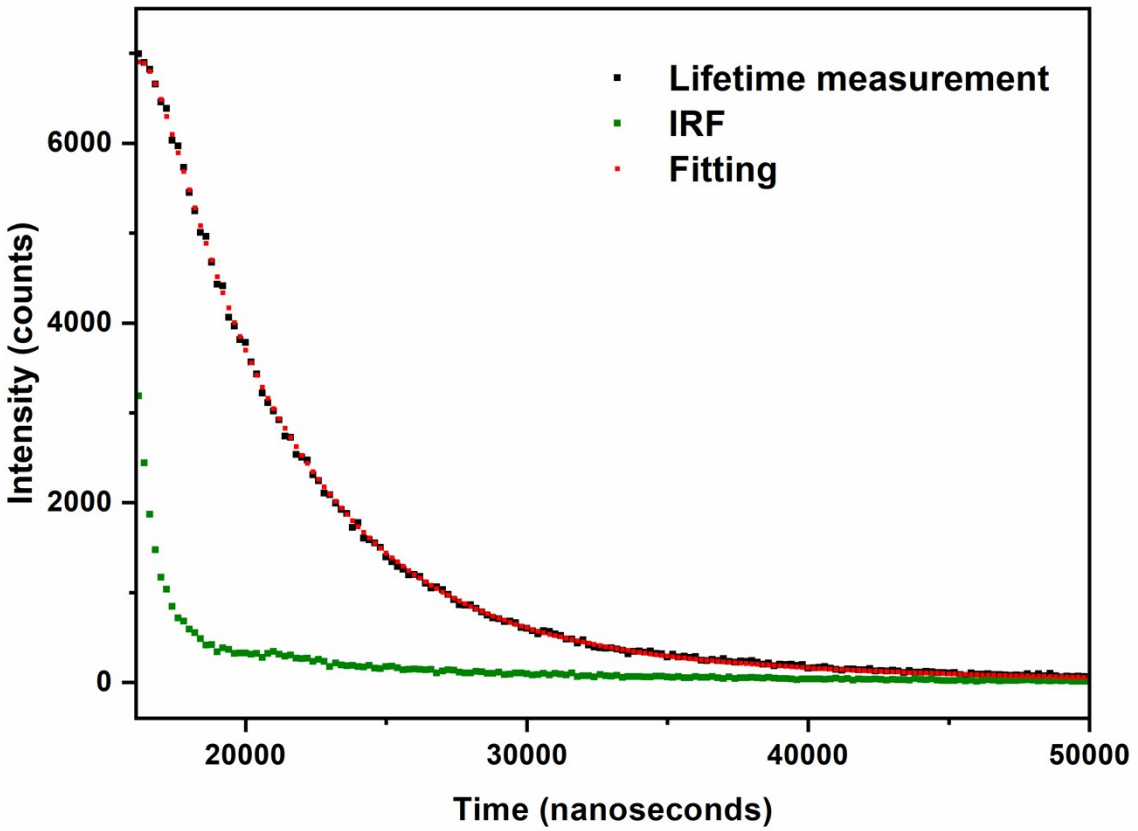

Figure S34. Lifetime decay for complex **4** at 77 K. *IRF (Instrumental Response Function) is used to detect the scattered light from the sample.

	Value	Std Dev		Value	Std Dev	Rel %
τ1	4.021E-6	1.338E-8	**B1**	1.173E-1	4.345E-4	100.00
<τ>amp	4.021E-6	1.338E-8				
Chisq	1.130		**A**	-2.427E-1		
Shift	3.495E-9					

- **Complex 5**

RT

Emission centred at 780 nm, excitation nanoled of 495 nm:

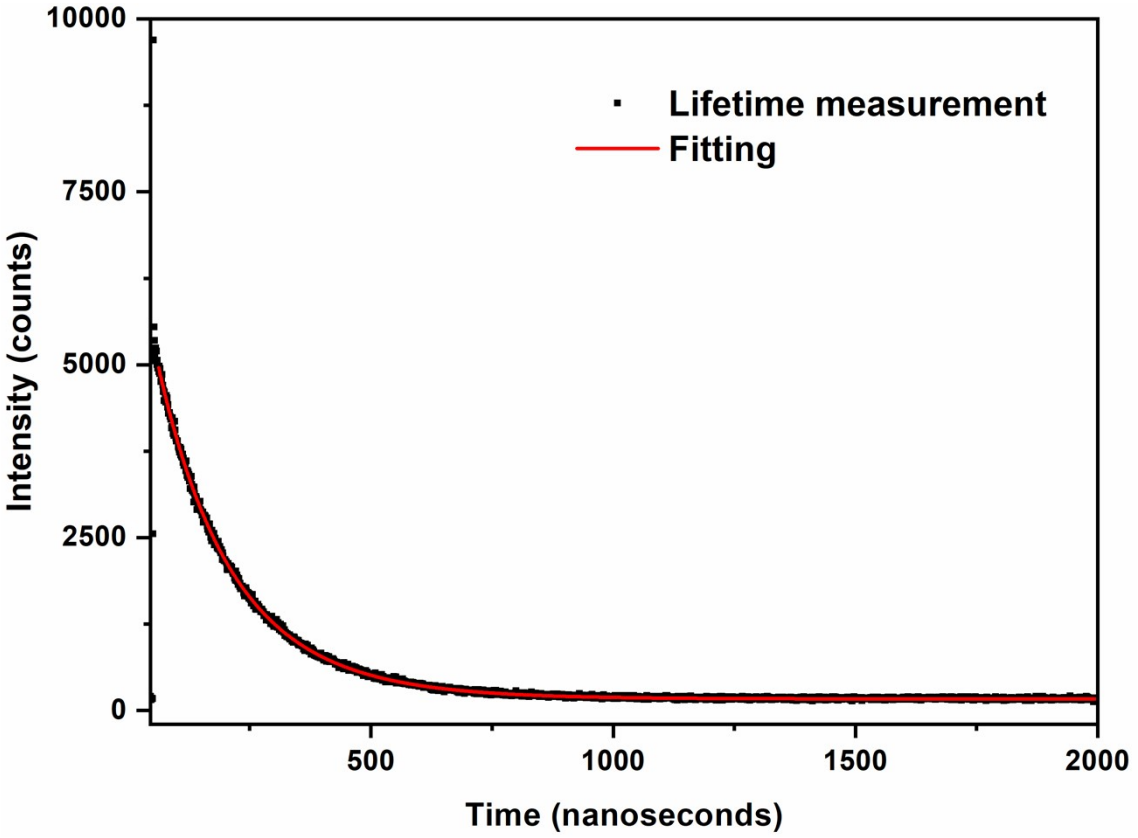

Figure S35. Lifetime decay for complex **5** at room temperature.

	Value	Std Dev		Value	Std Dev	Rel %
τ1	1.955E-7	1.644E-8	**B1**	1567.938	21.10683	22.39
τ2	3.293E-07	2.235E-08	**B2**	3225.583	14.12141	77.61
<τ>amp	0.286E-6					
Chisq	0.995		**A**	167.8747		
Shift	0					

II. Computational studies

1. Model systems

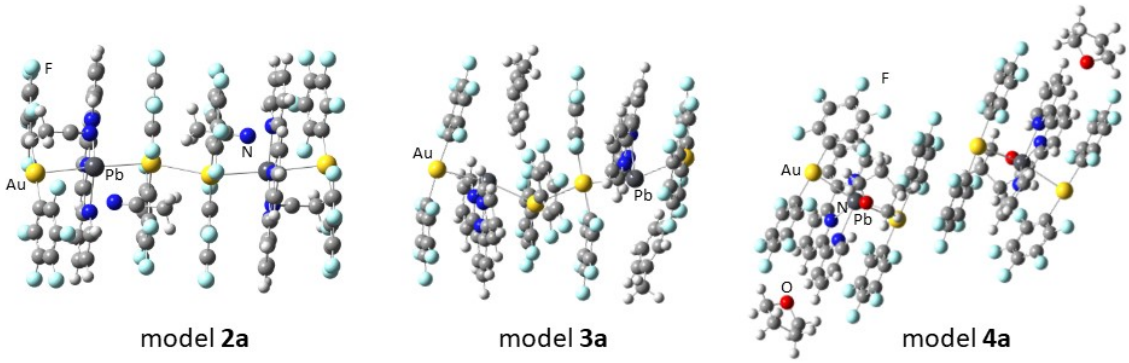

Figure S36. Representation of model systems **2a-4a**.

2. Population analysis

- Model system **2**

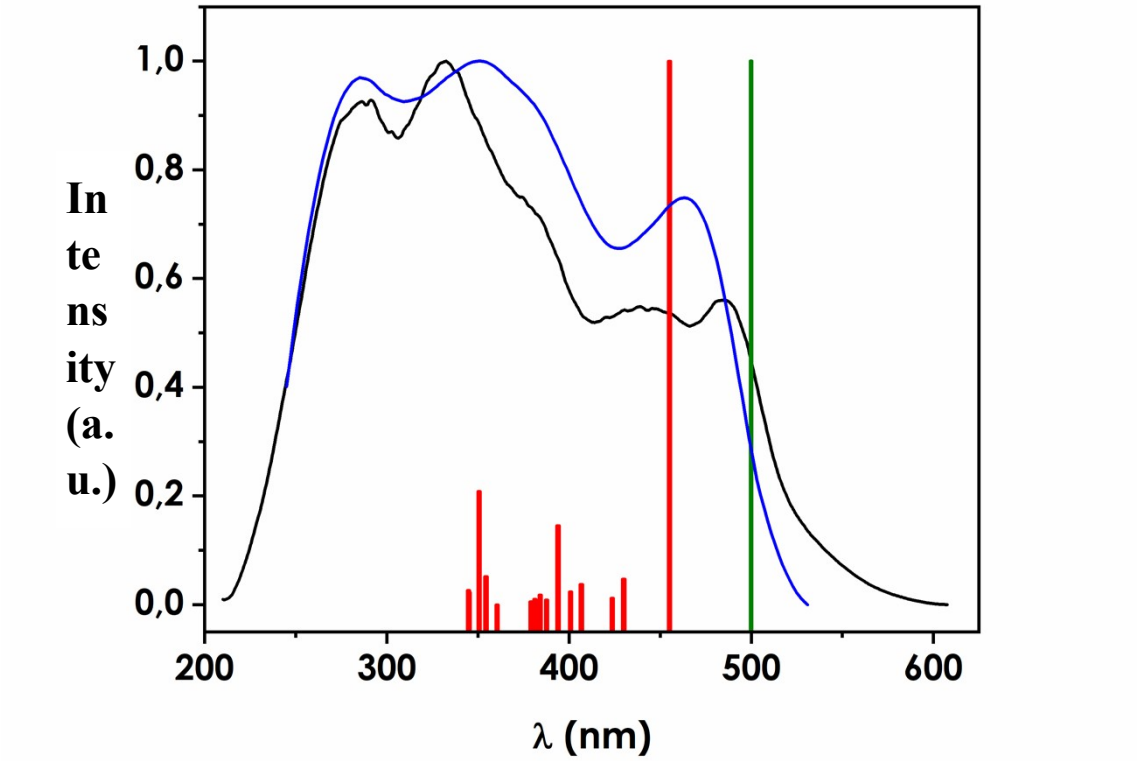

Figure S37. Comparison between solid-state UV-vis absorption spectra (black), theoretical singlet-singlet excitations (red) and theoretical singlet-triplet excitations (green) calculated from model **2a**.

Table S2. Population analysis for model system **2a**. Contribution from each part of the molecule to the orbitals involved in the most important transitions (%)

Orbital	Au	Pb	terpy	C_6F_5	CH_3CN
LUMO +1	4	8	80	0	0
LUMO	12	20	54	12	0
HOMO	62	10	2	24	0
HOMO -8	8	2	4	86	0
HOMO -9	4	0	8	86	0
HOMO -14	54	12	8	22	4

- Model system **3**

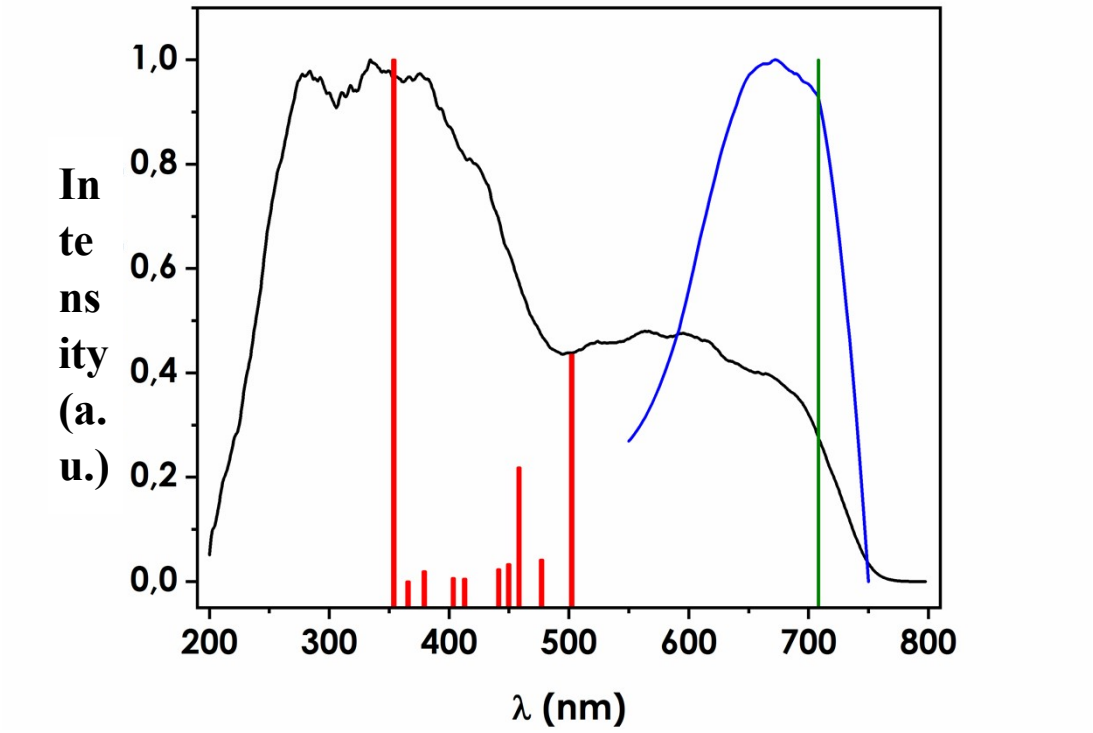

Figure S38. Comparison between solid-state UV-vis absorption spectra (black), theoretical singlet-singlet excitations (red) and theoretical singlet-triplet excitations (green) calculated from model **3a**.

Table S3. Population analysis for model system **3a**. Contribution from each part of the molecule to the orbitals involved in the most important transitions (%)

Orbital	Au	Pb	terpy	C_6F_5	Toluene
LUMO +4	19	31	35	16	0
LUMO +3	0	0	98	1	0
LUMO +2	0	0	98	2	0
LUMO +1	7	8	78	6	0
LUMO	8	12	72	9	0
HOMO	49	8	2	28	13

➢ Model system **4**

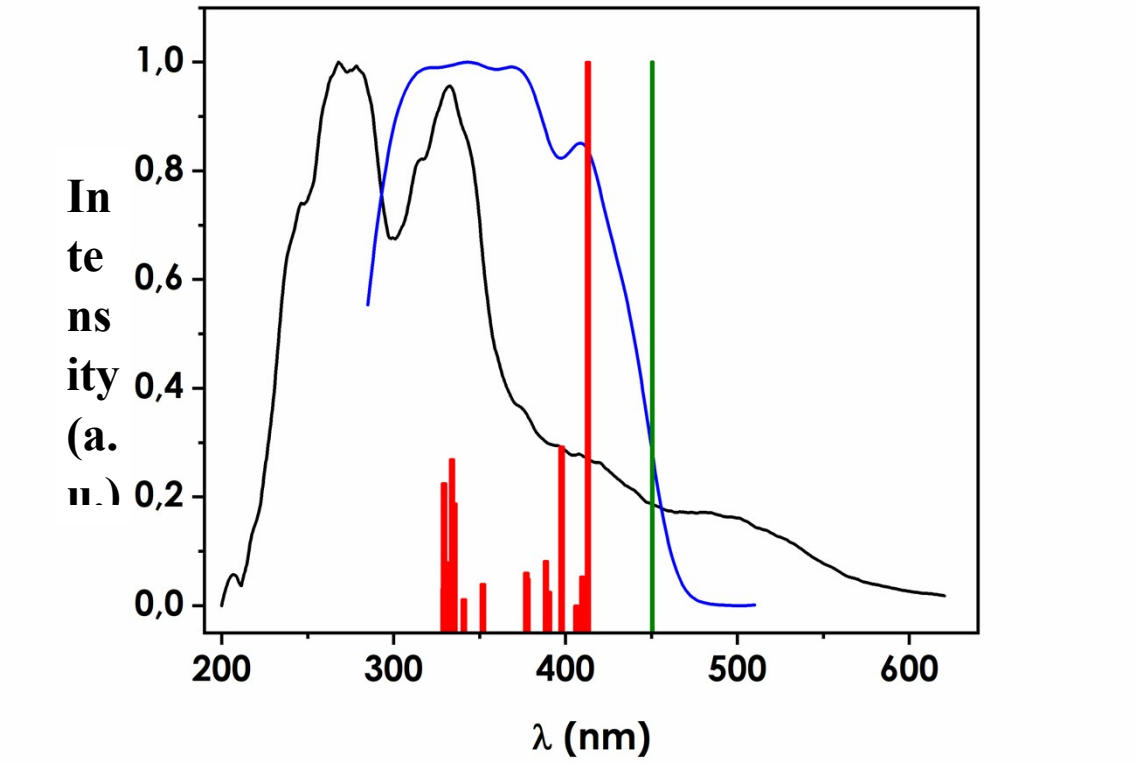

Figure S39. Comparison between solid-state UV-vis absorption spectra (black), theoretical singlet-singlet excitations (red) and theoretical singlet-triplet excitations (green) calculated from model **4a**.

Table S4. Population analysis for model system **4a**. Contribution from each part of the molecule to the orbitals involved in the most important transitions (%)

Orbital	Au	Pb	terpy	C_6F_5	THF
LUMO +3	0	1	97	2	0
LUMO +1	6	13	73	9	0
LUMO	8	13	70	8	0
HOMO	10	1	3	84	0
HOMO -1	29	4	3	62	2
HOMO -3	36	6	4	53	3
HOMO -5	40	7	3	43	3
HOMO -9	0	0	10	89	0
HOMO -19	3	0	78	20	0